

1 **An observational study of the effects of aerosols on diurnal variation of heavy rainfall**  
2 **and the concurrent cloud changes over Beijing-Tianjin-Hebei**

3  
4 Siyuan Zhou<sup>1</sup>, Jing Yang<sup>1,2\*</sup>, Wei-Chyung Wang<sup>3</sup>, Chuanfeng Zhao<sup>2,4</sup>, Daoyi Gong<sup>1,2</sup>, Peijun Shi<sup>1,2</sup>

5  
6 <sup>1</sup> Academy of Disaster Reduction and Emergency Management, Faculty of Geographical Science, Beijing  
7 Normal University, China

8 <sup>2</sup> State Key Laboratory of Earth Surface Process and Resource Ecology, Beijing Normal University, China

9 <sup>3</sup> Atmospheric Sciences Research Center, State University of New York, Albany, New York 12203, USA

10 <sup>4</sup> College of Global Change and Earth System Science, Beijing Normal University, China

11  
12  
13 Submitted to ACP

14 Oct 2018

15  
16  
17  
18  
19  
20  
21  
22  
23  
24  
25  
26  
27  
28  
29  
30  
31  
32 \*Correspondence to: Jing Yang, State Key Laboratory of Earth Surface Process and Resource  
33 Ecology/Academy of Disaster Reduction and Emergency Management, Faculty of Geographical Science,  
34 Beijing Normal University, 19#Xinjiekouwai Street, Haidian District, Beijing 100875, China. E-mail:  
35 yangjing@bnu.edu.cn

36 **Abstract:** Our previous study found that the observed rainfall diurnal variation over Beijing-Tianjin-Hebei  
37 shows distinct signature of the effects of pollutants. Here we used the hourly rainfall data together with  
38 satellite-based daily information of aerosols and clouds to further investigate the effects of aerosols on heavy  
39 rainfall, and the concurrent changes of cloud properties. For heavy rainfall, three distinguished characteristics  
40 are identified: *earlier start time*, *earlier peak time*, and *longer duration*. The quantitative values of these  
41 changes are however sensitive to the choice of pollution indicators: 0.7, 1.0 and 0.8 hours based on aerosol  
42 optical depth (AOD); and 2.1, 4.2 and 2.4 hours based on cloud droplet number concentration (CDNC).  
43 In-depth analysis suggests that the characteristics of earlier in both start time and peak time occur in the  
44 presence of black carbons (absorbing aerosols) while the longer duration is attributed to sulfates (scattering  
45 aerosols). Because of its close relevance to changes in heavy rainfall, we also examined changes of clouds.  
46 Significant increases in cloud fraction, cloud top pressure, the liquid/ice cloud optical thickness and cloud  
47 water path are found. However, changes in cloud microphysics show different responses between AOD and  
48 CDNC analyses. While decreases in ice cloud effective radius are found in both analyses, the liquid cloud  
49 effective radius is increased in AOD analysis but decreased in CDNC analysis. The effect of moisture (specific  
50 humidity at 850 hPa) on heavy rainfall and clouds was also studied and more moisture tends to increase  
51 rainfall duration. Finally, the mechanisms which may explain the aerosol effects are discussed and  
52 hypothesized.

53 **Key words:** aerosol, heavy rainfall, diurnal variation, cloud, Beijing-Tianjin-Hebei, observational study

54

## 55 **1. Introduction**

56 Aerosols modify the global hydrologic cycle through both radiative effect (direct effect) and cloud effect  
57 (indirect effect) (IPCC, 2013). On the one hand, through absorbing or scattering solar radiation, aerosols can  
58 lead to the air aloft heating (e.g. Jacobson 2001; Lau et al. 2006) or the surface cooling (Lelieveld and  
59 Heintzenberg 1992; Guo et al. 2013; Yang et al., 2018), which changes the atmospheric vertical static stability  
60 and modulates rainfall (e.g. Rosenfeld et al. 2008). On the other hand, water-soluble aerosols serving as cloud  
61 condensation nuclei (CCN) could affect the warm-rain processes and cold-rain processes through influencing  
62 the cloud droplet size distributions, cloud top heights and other cloud properties (Jiang et al., 2002; Givati and  
63 Rosenfeld 2004; Chen et al., 2011; Lim and Hong 2012; Tao et al., 2012). Beijing-Tianjin-Hebei (BTH) region  
64 is the heaviest aerosol polluted area in China and concerns have been raised about the  
65 aerosol-radiation-cloud-precipitation interaction over this region. The impact of aerosols on light rainfall or  
66 warm-rain processes over BTH region almost reaches consistent agreement (e.g., Qian et al., 2009), but  
67 aerosol effects on the heavy convective rainfall in this region still have large uncertainties (Wang et al., 2009;  
68 Guo et al., 2014; Wang et al., 2016).

69 The clouds that can generate heavy convective rainfall in BTH region usually contain warm clouds, cold

70 clouds and mixed-phase clouds (e.g. Guo et al., 2015). Because the aerosol-cloud interactions in different  
71 types of clouds are distinct (Gryspeerd et al., 2014), aerosol indirect effect during heavy rainfall is more  
72 complicated than its direct effect (Sassen et al., 1995; Sherwood, 2002; Jiang et al., 2008, Tao et al., 2012).  
73 For warm clouds, by serving as CCN that nucleates more cloud droplets, aerosols can increase cloud albedo so  
74 called albedo effect or Twomey effect (Twomey, 1977), lengthen the cloud lifetime so called lifetime effect  
75 (Albrecht, 1989), and enhance thin cloud thermal emissivity so called thermal emissivity effect (Garrett and  
76 Zhao, 2006). The above effects tend to increase the cloud microphysical stability and suppress warm-rain  
77 processes (Albrecht 1989; Rosenfeld et al. 2014). For cold clouds and mixed-phase clouds, many studies  
78 reported that the cloud liquid accumulated by aerosols is converted to ice hydrometeors above the freezing  
79 level, which invigorates deep convective clouds and intensifies heavy precipitation so called invigoration  
80 effect (Rosenfeld and Woodley, 2000; Rosenfeld et al., 2008; Lee et al. 2009; Guo et al. 2014). The Twomey  
81 effect infers that aerosols serving as CCN that increase the cloud droplets could reduce cloud droplet size  
82 within a constant liquid water path (Twomey, 1977). However, the opposite results of relationship between  
83 aerosols and cloud droplet effective radius were reported in observations (Yuan et al., 2008; Panicker et al.,  
84 2010; Jung et al., 2013; Harikishan et al., 2016; Qiu et al., 2017), which might be related with the moisture  
85 supply near the cloud base (Yuan et al., 2008; Qiu et al., 2017). Besides, the influence of aerosols on ice  
86 clouds also depends upon the amount of moisture supply (Jiang et al., 2008). Therefore, how the aerosols  
87 modify the heavy convective rainfall and concurrent cloud changes does not reach a consensus, particularly if  
88 considering the different moisture conditions.

89 Heavy convective rainfall over BTH region usually occurs within a few hours, thus studying on the  
90 relationship between aerosols and rainfall diurnal variation could deepen our understanding of aerosol effects  
91 on heavy rainfall. Several previous studies have found that aerosols are related to the changes of the rainfall  
92 diurnal variation in other regions (Kim et al., 2010; Gryspeerd et al., 2014; Fan et al., 2015; Guo et al., 2016;  
93 Lee et al., 2016). However, the above studies do not address the change of cloud properties and its sensitivity  
94 to different conditions of moisture supply. Although our recent work over BTH region (Zhou et al. 2018)  
95 attempted to remove the meteorological effect including circulation and moisture and found that the peak of  
96 heavy rainfall shifts earlier on the polluted condition, it only excluded the extreme moisture conditions and  
97 focused on aerosol radiative effect on the rainfall diurnal variation. Therefore, this study aims to deepen the  
98 previous study (Zhou et al., 2018) through investigating the following questions: (1) how do aerosols  
99 (including absorbing aerosols and scattering aerosols) modify the behaviors of the heavy rainfall diurnal  
100 variation (start time, peak time, duration and intensity)? (2) how do aerosols influence the concurrent cloud  
101 properties with inclusion of moisture? To solve above questions, we used aerosol optical depth (AOD) as a  
102 macro indicator of aerosol pollution and cloud droplet number concentration (CDNC) as a micro indicator of  
103 CCN served by aerosols respectively to compare the characteristics of heavy rainfall diurnal variation and the  
104 concurrent cloud properties between clean and polluted conditions, and applied aerosol index (AI) to  
105 distinguish the associated different effects of absorbing aerosols and scattering aerosols. In addition, we used

106 the specific humidity (SH) at 850 hPa as an indicator of moisture supply condition to investigate the possible  
107 effects of moisture on the rainfall and clouds and compared them with the effects of aerosols. The paper is  
108 organized as following: The data and methodology are introduced in Sect. 2. Section 3 addresses the  
109 relationship between aerosol pollution and diurnal variation of heavy rainfall, including the distinct  
110 characteristics of rainfall diurnal variation on clean/polluted conditions; the different behaviors of heavy  
111 rainfall diurnal variation along with the change of two different types of aerosols, and the comparison of  
112 heavy rainfall behaviors influenced respectively by moisture and aerosols. Section 4 describes the concurrent  
113 changes of cloud properties associated with pollution and examines the influences of CCN and moisture on  
114 the cloud properties. Section 5 makes a discussion on the distinct roles of aerosol radiative effect/cloud effect  
115 on the behaviors of heavy rainfall diurnal variation, as well as the uncertainties of different indicators and  
116 associated distinct results. Conclusion will be given in Sect. 6.

117

## 118 **2. Data and methodology**

### 119 **2.1 Data**

120 Four types of datasets from the year 2002 to 2012 (11 years) are used in this study, which include (1)  
121 precipitation, (2) aerosols, (3) clouds, and (4) other meteorological fields.

#### 122 **2.1.1 Precipitation data**

123 To study the diurnal variation of heavy rainfall, the gauge-based hourly precipitation datasets are used, which  
124 were obtained from the National Meteorological Information Center (NMIC) of the China Meteorological  
125 Administration (CMA) (Yu et al., 2007) at 2420 stations in China from 1951 to 2012. The quality control  
126 made by CMA/NMIC includes the check for extreme values (the value exceeding the monthly maximum in  
127 daily precipitation was rejected), the internal consistency check (wiping off the erroneous records caused by  
128 incorrect units, reading, or coding) and spatial consistency check (comparing the time series of hourly  
129 precipitation with nearby stations) [Shen et al., 2010]. Here we chose 176 stations in the plain area of BTH  
130 region that are below the topography of 100 meter above sea level as shown in Fig.1, because we purposely  
131 removed the probable orographic influence on the rainfall diurnal variation, which is consistent with our  
132 previous work (Zhou et al., 2018). The record analyzed here is the period of 2002 to 2012.

#### 133 **2.1.2 Aerosol data**

134 AOD is a proxy for the optical amount of aerosol particles in a column of the atmosphere and serves as one of  
135 indicators for the division of aerosol pollution condition in this study, which was obtained from MODIS  
136 (Moderate Resolution Imaging Spectroradiometer) Collection 6 L3 aerosol product with the horizontal  
137 resolution of  $1^{\circ} \times 1^{\circ}$  onboard the Terra satellite (Tao et al., 2015). The quality assurance of marginal or higher  
138 confidence is used in this study. The reported uncertainty in MODIS AOD data is on the order of (-0.02-10%),

139 (+0.04+10%) (Levy et al., 2013). The Terra satellite overpass time at the equator is around 10:30 local solar  
140 time (LST) in the daytime, and the satellite data is almost missing when it is rainy during the overpass time.  
141 As shown in Fig.2, the occurrence of selected heavy rainfall events in this study is mainly later than the  
142 satellite overpass time. Therefore, the AOD used here represents the situation of the air quality in advance of  
143 heavy rainfall appearance.

144 The ultraviolet AI from Ozone Monitoring Instrument (OMI) on board the Aura satellite which was  
145 launched in July 2004, is used for detecting the different types of aerosols in this study. The OMI ultraviolet  
146 AI is a method of detecting absorbing aerosols from satellite measurements in the near-ultraviolet wavelength  
147 region (Torres et al., 1998). The positive values of ultraviolet AI are attributed to the absorbing aerosols such  
148 as smoke and dust while the negative values of AI stand for the non-absorbing aerosols (scattering aerosols)  
149 such as sulfate and sea salt (Tariq and Ali, 2015). The near-zero values of AI occur when clouds and Rayleigh  
150 scattering dominate (Hammer et al., 2018). The horizontal resolution of AI data is  $1^{\circ}\times 1^{\circ}$  and it covers the  
151 period of 2005 to 2012.

152 MACC-II (Monitoring Atmospheric Composition and Climate Interim Implementation) reanalysis product  
153 produced by ECMWF (the European Centre for Medium-Range Weather Forecasts), provided the AOD  
154 datasets for different kinds of aerosols (BC, sulfate, organic matter, mineral dust and sea salt). MACC-II  
155 reanalysis products are observationally-based within a model framework, which can offer a more complete  
156 temporal and spatial coverage than observation and reduce the shortcomings of simulation that fail in  
157 simulating the complexity of real aerosol distributions (Benedetti *et al.*, 2009). The horizontal resolution of  
158 MACC-II is also  $1^{\circ}\times 1^{\circ}$  with the time interval of six-hour. MACC-II data covers the period of 2003 to 2012.

### 159 **2.1.3 Cloud data**

160 Daily cloud variables, including cloud fraction (CF), cloud top pressure (CTP), cloud optical thickness (COT,  
161 liquid and ice), cloud water path (CWP, liquid and ice) and cloud effective radius (CER, liquid and ice), were  
162 obtained from MODIS Collection 6 L3 cloud product onboard the Terra satellite. The MODIS cloud product  
163 combines infrared emission and solar reflectance techniques to determine both physical and radiative cloud  
164 properties (Platnick et al., 2017). The validation of cloud top properties in this product has been conducted  
165 through comparisons with CALIOP (Cloud-Aerosol Lidar with Orthogonal Polarization) data and other lidar  
166 observations (Holz et al., 2008; Menzel et al., 2008), and the validation and quality control of cloud optical  
167 products is performed primarily using in situ measurements obtained during field campaigns as well as the  
168 MODIS Airborne Simulator instrument (<https://modis-atmos.gsfc.nasa.gov/products/cloud>). Consistent with  
169 AOD, the measure of above cloud variables is before the occurrence of heavy rainfall.

170 CDNC is retrieved as the proxy for CCN and also another indicator for separating different aerosol  
171 conditions in this study. Currently, most derivations of CDNC assume that the clouds are adiabatic and  
172 horizontally homogeneous; CDNC is constant throughout the cloud's vertical extent, and cloud liquid water

173 content varies linearly with altitude adiabatically (Min et al., 2012; Bennartz and Rausch, 2017). According to  
174 Boers et al. (2006) and Bennartz (2007), we calculated CDNC (unit:  $\text{cm}^{-3}$ ) through:

$$175 \quad \text{CDNC} = \frac{C_w^{1/2}}{k} \frac{10^{1/2}}{4\pi\rho_w^{1/2}} \frac{\tau^{1/2}}{R_e^{5/2}} \quad (1)$$

176 Where  $C_w$  is the moist adiabatic condensate coefficient, and its value depends slightly on the temperature  
177 of the cloud layer, ranging from 1 to  $2.5 \times 10^{-3} \text{ gm}^{-4}$  for a temperature between 0 °C and 40 °C (Brenquier,  
178 1991). In this study, we calculated the  $C_w$  through the function of the temperature (see Fig.1 in Zhu et al.,  
179 2018) at a given pressure that is 850 hPa. And we have tested the sensitivity of CDNC to the amount of  $C_w$   
180 and found it almost keeps the same when the  $C_w$  changes from 1 to  $2.5 \times 10^{-3} \text{ gm}^{-4}$ . The coefficient k is the  
181 ratio between the volume mean radius and the effective radius and varies between 0.5 and 1 (Brenquier et al.,  
182 2000). Here we used  $k = 1$  for that we cannot get the accurate value of k and the value of k does not influence  
183 the rank of CDNC for the division of aerosol condition in this study.  $\rho_w$  is cloud water density.  $\tau$  and Re are  
184 the liquid COT and CER obtained from MODIS Collection 6 L3 cloud product onboard the Terra satellite. To  
185 reduce the uncertainty of CDNC retrieval caused by the heterogeneity effect from thin clouds (Nakajima and  
186 King, 1990; Quaas et al., 2008; Grandey and Stier, 2010; Grosvenor et al., 2018), we selected the CF more  
187 than 80%, the liquid COD more than 4 and the liquid CER more than  $4 \mu\text{m}$  when calculating the CDNC  
188 (Quaas et al., 2008).

#### 189 **2.1.4 Other meteorological data**

190 Other meteorological factors, including wind, temperature, pressure and SH, were obtained from the  
191 ERA-Interim reanalysis datasets with  $1^\circ \times 1^\circ$  horizontal resolution and 37 vertical levels at six-hour intervals.  
192 ERA-Interim is a global atmospheric reanalysis produced by ECMWF, which covers the period from 1979 to  
193 near-real time (Dee et al., 2011). The SH, which stands for the water vapor content, serves as the indicator of  
194 moisture supply condition in this study.

195

## 196 **2.2 Methodology**

### 197 **2.2.1 Method of interpolation**

198 We used both station data of gauge-based precipitation and gridded data including aerosols, clouds and other  
199 meteorological variables. Gridded datasets in this study were downloaded with the horizontal resolution of  
200  $1^\circ \times 1^\circ$ , which are consistent with the resolution of MODIS L3 product. To unify the datasets, we interpolated  
201 all the gridded datasets onto the selected 176 rainfall stations using the average value in a  $1^\circ \times 1^\circ$  grid as the  
202 background condition of each rainfall station, i.e., the stations in the same  $1^\circ \times 1^\circ$  grid have the same aerosol,  
203 cloud and meteorological conditions.

### 204 **2.2.2 Selection of sub-season and circulation**

205 Consistent with our previous work, we focused on early summer (1 June to 20 July) before the large-scale  
206 rainy season starts, in order to remove the large-scale circulation influence and identify the effect of aerosols on  
207 local convective precipitation because BTH rainfall during this period is mostly convective rainfall (Yu et al.,  
208 2007) with heavy pollution (Zhou et al., 2018). And to unify the background atmospheric circulation, we only  
209 selected the rainfall days with southwesterly flow, which is the dominant circulation accounting for 40% of  
210 total circulation patterns over the BTH region during early summer (Zhou et al., 2018).

### 211 **2.2.3 Classification of the heavy rainfall, clean/polluted and moisture conditions**

212 With the circulation of southwesterly, we selected heavy rainfall days when the hourly precipitation amount is  
213 more than 8.0 mm/hour (defined by *Atmospheric Sciences Thesaurus, 1994*). Here “a day” is counted from 8  
214 LST to 8 LST next day (0 UTC to 24 UTC). We used two indicators to distinguish the clean and polluted  
215 conditions, which are AOD and CDNC. The 25<sup>th</sup> and 75<sup>th</sup> AOD/CDNC of the whole rainfall days are used as  
216 the thresholds of clean and pollution condition, and the values are shown in Tab.1. It shows that there are 514  
217 cases of heavy rainfall on polluted days and 406 cases of that on clean days when using AOD, and 630/716  
218 cases on polluted/clean condition when using CDNC.

219 The absorbing aerosols are detected using the positive values of AI that is named as absorbing aerosol index  
220 (AAI) here, and we can retrieve the scattering aerosol index (SAI) using the negative values of AI. AAI and  
221 SAI are also divided into two groups using the threshold of 25<sup>th</sup>/75<sup>th</sup> as shown in Tab.1. We used AAI/SAI  
222 more than 75<sup>th</sup> as the extreme circumstances of absorbing aerosols and scattering aerosols to compare their  
223 impacts on heavy rainfall. The case numbers are 375 and 550 respectively for the extreme AAI and SAI cases.  
224 Using the same method, we chose cases with more BC/sulfate when the AOD of BC/sulfate is larger than the  
225 75<sup>th</sup> of itself in all rainy days, and cases with less BC/sulfate when that is less than the 25<sup>th</sup> of itself in the same  
226 condition. Accordingly, we selected 459 cases with more BC and 274 cases with less BC with heavy rainfall.  
227 Similarly, 361 cases with more sulfate and 419 cases with less sulfate with heavy rainfall were selected.

228 The SH at 850 hPa is used as the indicator of moisture supply under the cloud base. We chose wet cases  
229 when the SH on that rainy day is larger than 75<sup>th</sup> tercile of the whole rainy days, and chose dry cases when SH  
230 on that day is less than the 25<sup>th</sup> tercile of the whole rainy days (the thresholds are shown in Tab. 1).

### 231 **2.2.4 Statistical analysis**

232 We adopted the probability distribution function (PDF) to compare the features of heavy rainfall and cloud  
233 variables on different conditions of aerosols, through which we can understand the changes of rainfall/cloud  
234 properties more comprehensively. The numbers of bins we selected in the study have been all tested for better  
235 representing the PDF distribution. Student’s t-test is used to examine the significance level of differences  
236 between the different groups of aerosol conditions.

237

### 238 **3. Relationship between aerosol pollution and diurnal variation of heavy rainfall over BTH**

#### 239 **3.1 Distinct characteristics of heavy rainfall diurnal variation associated with aerosol pollution**

240 Our previous study (Zhou et al. 2018) has reported the distinct peak shifts of rainfall diurnal variation between  
241 clean and polluted days using the indicator of AOD over the BTH region during early summer. Similar with  
242 our previous study, the PDF of the heavy rainfall peak time shows that the maximum of rainfall peak is about  
243 two hours earlier on the polluted days (20:00 LST) than that on the clean days (22:00 LST) (Fig. 2a). To  
244 comprehensively recognize the changes of rainfall diurnal variation associated with air qualities, here we  
245 examined the PDF of the start time, the duration and the intensity besides the peak time of heavy rainfall.

246 As shown in Fig. 2a, the start time of heavy rainfall exhibits a significant advance on the polluted days. The  
247 secondary peak on the early morning is ignored here because the early-morning rainfall is usually associated  
248 with the mountain winds (Wolyn et al., 1994; Li et al., 2016) and the nighttime low-level jet (Higgins et al., 1997;  
249 Liu et al., 2012) that is beyond the scope of this study. The time for the maximum frequency of heavy rainfall  
250 initiation is 6 hours earlier on the polluted days, shifting from around 0:00 LST on the clean days to the 18:00  
251 LST (Fig. 2a). Regarding the rainfall durations, the average persistence of heavy rainfall on polluted days is  
252 0.8 hours longer than that on clean days (Tab. 2). According to the PDF shown as in Fig. 2a, the occurrence of  
253 short-term precipitation ( $\leq 6$  hours, Yuan et al., 2010) decreases while that of long-term precipitation ( $> 6$  hours,  
254 Yuan et al., 2010) increases. The intensity of hourly rainfall exhibits a non-significant increase on the polluted  
255 days.

256 The distinct behaviors of heavy rainfall diurnal variation between clean and polluted days have been well  
257 demonstrated using the indicator of AOD. However, AOD is not a proper proxy for CCN (Shinozuka et al.,  
258 2015) but the property of aerosols serving as CCN should be considered because aerosol-cloud interaction  
259 plays an indispensable role on changing rainfall diurnal variation. Therefore, here we applied the retrieved  
260 CDNC as the indicator of CCN (Zeng et al., 2014; Zhu et al., 2018) to examine the above-mentioned results.  
261 As a result, the similar changes of heavy rainfall can be well exhibited in CDNC analysis as shown in Fig. 2b.  
262 The start time and peak time of heavy rainfall on the polluted condition also show significant advances  
263 compared with that on the clean condition, with the average advances of 1.4 hours and 3.0 hours respectively  
264 (Tab. 2). The duration of heavy rainfall on the polluted condition is also prolonged, which is 2.2 hours longer  
265 in average (Tab. 2). Similar with the results based on AOD, the difference of rainfall intensity between clean  
266 and polluted conditions using CDNC does not pass the 95% statistical confidence level as well.

267 Hence, the results using either AOD or CDNC show that the start and peak time of heavy rainfall occur  
268 earlier and the duration becomes longer under pollution, although there are some quantitative differences  
269 between the two indicators. Since the difference of rainfall intensity is not significant in this study, the  
270 following analysis only focuses on studying the start time, peak time and duration of heavy rainfall along with  
271 aerosol pollution.



272

### 273 **3.2 Distinct behaviors of heavy rainfall diurnal variation associated with two different types of aerosols**

274 Using the indicator of AI, we further investigated distinct behaviors of heavy rainfall diurnal variation related  
275 to absorbing aerosols and scattering aerosols respectively. The PDF of start time, peak time and duration of  
276 heavy rainfall under the extreme circumstances of absorbing aerosols and scattering aerosols are compared in  
277 Fig. 3. Here, we briefly named the days with extreme large amount of absorbing aerosols as absorbing aerosol  
278 days and with more scattering aerosols as scattering aerosol days. The start time of heavy rainfall on  
279 absorbing aerosol days shows a significant earlier compared with that on scattering aerosol days (Fig. 3a),  
280 with 0.7 hours advance in average (Tab. 3). Similarly, the rainfall peak time also shows earlier on absorbing  
281 aerosol days (Fig. 3b), with an average advance of 1.6 hours (Tab. 3). The rainfall duration on scattering  
282 aerosol days shows longer than that on absorbing aerosol days, which are 6.0 hours and 5.0 hours respectively  
283 in average (Tab. 3). All the above-mentioned differences between the two groups have passed 95% statistical  
284 confidence level. The results indicate that the absorbing aerosols and scattering aerosols may have different or  
285 inverse effects on the heavy rainfall that absorbing aerosols may generate the heavy rainfall in advance while  
286 the scattering aerosols may delay and prolong the heavy rainfall.

287 To further verify the different behaviors of heavy rainfall diurnal variation associated with two different  
288 types of aerosols, we purposely re-examine the above-mentioned phenomena using BC/sulfate that can  
289 represent typical absorbing/scattering aerosols over the BTH region. BC has its maximum center over BTH  
290 region (Fig. 4a) and our previous study has indicated that the radiative effect of BC low-level warming may  
291 facilitate the convective rainfall generation (Zhou et al., 2018). The percentage of sulfate is also large over the  
292 BTH region (Fig. 4b) and the sulfate is one of the most effective CCN that influences the precipitation in this  
293 region (Gunthe et al., 2011). Accordingly, we selected the cases with different amounts of BC and sulfate  
294 AOD to compare their roles on the diurnal variation of heavy rainfall. The methods have been described in  
295 Sect. 2.2.3. The PDF of the start time, peak time and duration of heavy rainfall in the cases with higher and  
296 lower amount of BC are shown in Fig. 5a, respectively. The most striking result is that the maximum  
297 frequency of rainfall start time in high BC cases evidently shifts earlier (Fig. 5a). Meanwhile, the mean peak  
298 time in high BC cases shows 1.1 hour earlier than that in low BC cases (Tab. 3). And the duration of heavy  
299 rainfall is slightly shortened by the averaged 0.2 hours in high BC cases. The features in high BC cases are  
300 consistent with the above absorbing aerosol effect. In contrast, when the sulfate has higher amount, the mean  
301 start time of rainfall is delayed by 0.5 hours, while the duration shows a significant increase by 1.5 hours in  
302 average (Tab. 3). The behaviors in high sulfate cases also exhibit similar with the above scattering aerosol  
303 effect, except for the peak time that shows later in scattering aerosols but a little earlier in high sulfate cases  
304 (Tab. 3).

305

306 **3.3 Behavior comparisons of heavy rainfall diurnal variation influenced by moisture and aerosol.**

307 Moisture supply is an indispensable factor for the precipitation formation. Since the southwesterly circulation  
308 can not only transport pollutants but also plenty of moisture to the BTH region (Wu et al., 2017), more  
309 pollution usually corresponds to more moisture for the BTH region (Sun et al., 2015) so that it is hard to  
310 completely remove the moisture effect on the above results in the pure observational study. Here we attempt  
311 to recognize the moisture effect on the heavy rainfall to further understand the above aerosol-associated  
312 changes. Because the moisture supply for BTH is mainly transported via low-level southwesterly circulation,  
313 we purposely used the SH at 850 hPa as the indicator of moisture condition.

314 Using the similar percentile method with polluted/clean days, we got the rainfall characteristics in more  
315 humid (more than 75<sup>th</sup> tercile) and less humid (less than 25<sup>th</sup> tercile) environments on the heavy rainfall days  
316 regardless of the aerosol condition, as shown in Fig. 6a. The results show the start time of heavy rainfall is  
317 delayed by 0.9 hours, the peak time is 0.6 hour earlier and the duration is prolonged by 2.0 hours in average in  
318 the more humid environment, which is similar with the result on the condition of more sulfate. Besides, the  
319 same results are obtained with different moisture indicator, e.g. the 850 hPa absolute humidity. These results  
320 indicate the advance of heavy rainfall start time on polluted days is not caused by more moisture supply, while  
321 the longer duration and earlier peak in high sulfate cases might be related to the increased moisture supply.

322 We also investigate the characteristics of low-level moisture and rainfall behavior distribution in clean and  
323 polluted cases respectively using AOD and CDNC (Fig. 6 b&c). The results show that the relationship  
324 between moisture and rainfall start time/peak time/duration is not linear. Using either AOD or CDNC, the  
325 distribution of SH exhibits a slight increase in polluted cases, indicating that the polluted cases have more  
326 moisture than the clean cases which is particularly well shown using AOD. However, when fixing the  
327 moisture at a certain range especially at the relative dry condition, we can detect the similar phenomena of  
328 earlier start/peak time and longer duration in polluted cases. For example, when the amount of 850 hPa SH is  
329 between 8-12 g/kg, the start & peak time in polluted cases show significant earlier and the duration exhibits  
330 slightly increased compared with that in clean cases.

331 The above results indicate that the advance of heavy rainfall start and peak time in polluted cases might be  
332 weakly related to the moisture effect, but the moisture could obviously prolong the duration of heavy rainfall  
333 (Fig. 6a). Because the diurnal change of heavy rainfall with more moisture is similar with the behaviors of  
334 heavy rainfall with scattering aerosols especially sulfate, we cannot figure out their individual role in this  
335 section.

336

337 **4 Relationship between aerosol pollution and concurrent changes of cloud properties associated with**  
338 **heavy rainfall diurnal variation**

339 **4.1 Concurrent changes of cloud properties along with heavy rainfall diurnal variation on clean and**

340 **polluted conditions**

341 To understand the cloud effect of aerosols during heavy rainfall diurnal variation, we need to recognize the  
342 concurrent cloud characteristics on clean and polluted conditions. The cloud properties we used were obtained  
343 from satellite product that were measured at the same time with aerosols before the occurrence of heavy  
344 rainfall. The differences of cloud features were examined in both macroscopic (including CF, CTP, COT and  
345 CWP) and microscopic properties (including CER) between the clean and polluted conditions based on AOD  
346 and CDNC respectively, as shown in Fig. 7.

347 Using AOD as the pollution indicator, the PDF distribution of CF shows that the CF on the polluted  
348 condition is evidently larger than that on the clean condition. The average CF is 62.8% on the clean condition,  
349 and 89.3% on the polluted condition, which increases 42.2% (Tab. 4). The average CTP on the polluted  
350 condition is 487.3 hPa, which is larger than 442.3 hPa on the clean condition and increases 10.2%, indicating  
351 that the cloud top height is lower on the polluted days. The COT, CWP and CER were further analyzed for the  
352 liquid and ice portions of clouds as shown in Fig. 7. Both liquid and ice COT on polluted condition exhibit  
353 significant increases compared with that on clean condition. The mean amount of liquid COT is increased by  
354 44.9% and ice COT increases by 92.5% (Tab. 4). Similar with COT, the amount of liquid and ice CWP also  
355 increase on polluted condition, which increase by 53.5% and 71.6% respectively. In addition, the liquid CER  
356 is increased by 4.8% and the ice CER is decreased by 8.8% on the polluted days. The differences of above  
357 cloud properties between clean and polluted cases have all passed the 95% statistical confidence level.

358 Using CDNC as another pollution indicator, the above-mentioned changes of cloud properties are consistent  
359 with that using AOD, except for liquid CER (Fig. 7). The PDF of liquid CER on the polluted condition shifts  
360 to larger size based on AOD but smaller size based on CDNC. The inconsistency of liquid CER using two  
361 indicators might be due to the calculation method of CDNC which is not independent on the CF, liquid COD  
362 and liquid CER. But according to other variables that are independent of the CDNC calculation, we found the  
363 cases with more CDNC are accompanied with the increase of CTP, ice COT and liquid & ice CWP, which  
364 increase by 8.2%, 280.5%, 210.7% and 216.1% respectively (Tab 4) and all of which are consistent with the  
365 results based on AOD. The CER of ice clouds also shows a consistent decrease by 25.7% on the polluted  
366 condition based on CDNC. We noticed that the changes of the COT/CWP/CER for both liquid and ice based  
367 on CDNC are much larger than that based on AOD, which indicates that these cloud properties might be more  
368 sensitive to the indicator of CDNC rather than AOD.

369 According to the above comparison, the concurrent changes of cloud properties along with heavy rainfall  
370 diurnal variation show consistent results using the two pollution indicators (AOD and CDNC). The pollution  
371 corresponds to the increase of CF, COT and CWP both for liquid and ice, but the decrease of cloud top height  
372 (the increase of CTP corresponds to the decrease of cloud top height) and ice CER. The changes of liquid  
373 CER are opposite between the two indicators, but it might be due to the potential negative correlation between  
374 liquid CER and CDNC in the CDNC retrieval. Since we cannot distinguish the liquid part of mix-phased

375 clouds from liquid (warm) clouds in the observation, the changes of liquid cloud properties above might come  
376 from both the liquid (warm) clouds and the liquid part of mixed-phase clouds. Likewise, the above-mentioned  
377 changes of ice cloud properties might come from both ice (cold) clouds and the ice part of mixed-phase  
378 clouds.

379

#### 380 **4.2 Influences of CCN and moisture on the cloud properties**

381 Section 3.3 has shown that the diurnal variation of heavy rainfall with more moisture supply is similar with  
382 the changes of heavy rainfall with more sulfate aerosol. We assume that the moisture under the cloud base and  
383 the sulfate serving as CCN both influence the cloud properties (Yuan et al., 2008; Jiang et al., 2008; Jung et al.,  
384 2013; Qiu et al., 2017). To identify the effect of aerosols on clouds and its sensitivity to moisture, we  
385 purposely investigated the changes of above cloud properties with different conditions of the CDNC and the  
386 low-level moisture (850hPa SH) respectively. We categorized all cases of heavy rainfall into four groups,  
387 which are (1) clean and dry, (2) polluted and dry, (3) clean and wet, (4) polluted and wet, and checked the  
388 changes of above cloud properties, as shown in Tab. 5. To retrieve the comparable samples, here  
389 “clean/polluted” refers to the CDNC on that rainfall day less/more than 25<sup>th</sup>/75<sup>th</sup> tercile of the CDNC among  
390 the heavy rainfall days, and similarly, the “dry/wet” refers to the SH on that rainfall day less/more than  
391 25<sup>th</sup>/75<sup>th</sup> tercile of itself among the heavy rainfall days. The average CDNC is 2168.7 cm<sup>-3</sup> on the dry condition  
392 and 2168.1 cm<sup>-3</sup> on the wet condition, and the average SH is 11.3 g/kg and 11.8 g/kg on the clean and polluted  
393 conditions respectively, thus we can consider the CDNC or SH remain the same when the other condition  
394 changes. We made the significant test of differences between group 1 and 2, group 1 and 3, group 2 and 4,  
395 group 3 and 4. Because the CF is fixed above 80% when calculating the CDNC (see in Sect. 2.1.3), here the  
396 selected groups all belong to the condition of higher CF.

397 Comparing the results of group 1 and 2, which are both on the dry condition, we can identify the influence  
398 of CDNC on cloud properties. The changes of these cloud variables are the same as that in Sect. 5.1, that the  
399 CF, COT and CWP both for liquid and ice are increased on the polluted condition, while the cloud top height  
400 and liquid & ice CER are decreased based on CDNC. Among these variables, the liquid & ice COT and CWP  
401 are especially larger on the polluted condition, which are 5-6 times larger than that on the clean condition. The  
402 liquid CER on polluted condition also changes evidently, which becomes almost a half of that on clean  
403 condition. On the wet condition, comparing the group 3 and 4, the changes are similar that the CF, COT and  
404 CWP both for liquid and ice are increased and the liquid and ice CER are decreased but the change of CTP  
405 becomes not significant. However, the changes of these variables on the dry condition are evidently enhanced  
406 than that on the wet condition, which indicates these cloud properties might be more sensitive to the CDNC on  
407 the dry condition. The above comparisons indicate that with the increase of CDNC (which stands for CCN),  
408 the CF, COT and CWP are increased while the CER is decreased for both liquid and ice clouds regardless of  
409 the moisture amount.

410 Comparing the results of group 1 and 3, we can get the changes of cloud properties related only to moisture  
411 on the same clean condition. A common feature is that CTP, COT and CWP both for liquid and ice exhibit  
412 increases along with the increase of moisture. Compared with the CTP on the clean and dry condition, it  
413 increases on both polluted & dry condition (group 2) and clean & wet condition (group 3), but on the former  
414 condition its increase is larger, which indicates the influence of moisture on CTP might be secondary  
415 compared to the CDNC effect. Similarly, comparing the COT/CWP in group 2 and 3, the increases of COT  
416 and CWP both for liquid and ice in group 2 are 3-6 times larger than that in group 3, which indicates that the  
417 influences of moisture on COT and CWP does not overcome the influence of CCN. The change of liquid CER  
418 is not significant on the same clean condition, but the ice CER is significantly decreased with the increase of  
419 moisture. On the polluted condition, comparing group 2 and 4, we found the COT and CWP both for liquid  
420 and ice on the wet condition are evidently smaller than that on the dry condition, which indicates that  
421 increasing the moisture might partly compensate for the influence of CDNC on COT/CWP.

422 The results above indicate that both CCN and moisture have impacts on cloud properties. They both  
423 contribute to the increase of CF, COT and CWP, in which the influence of CCN on COT and CWP are  
424 significantly larger than moisture. The increase of either CCN or moisture corresponds to the increase of CTP.  
425 But when the CCN and moisture increase simultaneously, the CTP becomes smaller. Both CCN and moisture  
426 correspond to the decrease of ice CER, while only CCN corresponds to the significant decrease of liquid CER  
427 and that might be ascribed to the calculation method of CDNC. To reduce uncertainties, we have tested the  
428 SH at different levels (e.g., 700 hPa and 800 hPa) and different moisture indicator (e.g. absolute humidity) to  
429 verify above results, and found most cloud variables show the similar changes with the above except for the  
430 CTP and the liquid CER, which indicates the changes of CTP and liquid CER are more sensitive and have  
431 larger uncertainties. Since the behaviors of cloud changes are similar along with the increase of either CDNC  
432 or moisture but more sensitive to the former, the results in Sect. 5.1 might actually reflect the combined effect  
433 of CCN and moisture, and the aerosol effect on these cloud properties might be dominant on the polluted  
434 days.

435

## 436 **5. Discussion**

### 437 **5.1 Different roles of aerosol radiative effect and cloud effect in heavy rainfall**

438 In Sect. 3 we found that the heavy rainfall has earlier start time and peak time, and longer duration on the  
439 polluted condition. And afterwards, the earlier start of rainfall under pollution was found related to absorbing  
440 aerosols mainly referring to BC (Fig. 3a&5a). We also compared the effect of BC on the associated clouds.  
441 Figure 8a shows the CF larger than 90% rarely occurs in high BC environment, which might be associated  
442 with the semi-direct effect of BC (IPCC, 2013) or estimated inversion strength and BC covary. This result  
443 indicates the influence of BC on the heavy rainfall in Fig. 5a is mainly due to the radiative effect rather than

444 the cloud effect. The mechanism of BC effect on the heavy rainfall can be interpreted by our previous study  
445 (Zhou et al., 2018) as: BC absorbs shortwave radiation during the daytime and warms the lower troposphere at  
446 around 850 hPa, and then increases the instability of the lower to middle atmosphere (850-500hPa) so that  
447 enhances the local upward motion and moisture convergence. As a result, the BC-induced thermodynamic  
448 instability of the atmosphere triggers the occurrence of heavy rainfall in advance. Thus, the low-level heating  
449 effect of BC might play a dominant role in the beginning of rainfall especially before the formation of clouds  
450 during the daytime.

451 The delayed start of heavy rainfall with scattering aerosols in Fig. 3a and higher sulfate in Fig. 5b is  
452 consistent with many studies that both the radiative effect and cloud effect of sulfate-like aerosols could delay  
453 or suppress the occurrence of rainfall (Guo et al., 2013; Wang et al., 2016; Rosenfeld et al. 2014). Sulfate-like  
454 aerosols as scattering aerosols could prevent the shortwave radiation from arriving at the surface thus cool the  
455 surface and stabilize the atmosphere, which suppresses the rainfall formation (Guo et al., 2013; Wang et al.,  
456 2016). Sulfate-like aerosols serving as CCN can also suppress the rainfall by cloud effect through reducing the  
457 cloud droplet size and thus suppressing the collision-coalescence process of cloud droplets (Albrecht 1989;  
458 Rosenfeld et al. 2014). Figure 8b does shows that in contrast with BC, the CF larger than 90% is significantly  
459 increased in the high sulfate environment, which indicates the sulfate-like aerosols might have more evident  
460 influence on the clouds and subsequently the rainfall changes associated with sulfate are probably due to the  
461 cloud effects. Another significant feature is the longer duration of heavy rainfall in both the scattering aerosol  
462 cases and high sulfate cases (Fig 3c&5b). Since the heavy rainfall shows the similar changes with the increase  
463 of sulfate and moisture, we currently cannot separate their respective roles in this study. We speculate that the  
464 postponed start of heavy rainfall is mainly due to the effect of sulfate-like aerosols. While the longer duration  
465 is caused by both the cloud effect of sulfate-like aerosols and the increased moisture supply, because  
466 increasing either CCN or the moisture supply can increase cloud water (Sect. 4.2), which could lead to the  
467 longer rainfall duration. To further investigate the mechanism of longer duration, we need the assistance of  
468 numerical model simulations in the future work.

469 Accordingly, we speculate that the earlier start time of heavy rainfall related to absorbing aerosols (BC) is  
470 due to the radiative heating effect of absorbing aerosols, while the longer rainfall duration is probably caused  
471 by both the cloud effect of sulfate-like aerosols and the increased moisture supply. As a summary we use a  
472 schematic diagram (Fig. 9) to illustrate how aerosols modify the heavy rainfall over the BTH region. On one  
473 hand, BC heats the lower troposphere, changing the thermodynamic condition of atmosphere, which increases  
474 upward motion and accelerates the formation of cloud and rainfall. On the other hand, the increased upward  
475 motion transports more sulfate-like particles and moisture into the clouds so that more CCN and sufficient  
476 moisture increase the cloud water, thus might prolong the duration of rainfall. As a result, the heavy rainfall  
477 over BTH region in southwesterly shows earlier start and peak time, and longer duration might due to the  
478 combined effect of aerosol radiative effect, aerosol cloud effect as well as moisture effect. To further  
479 distinguish the individual effect, we need to conduct numerical model simulations in our future study.

480

## 481 **5.2 Uncertainties of different indicators and associated distinct results**

482 The gauge-based hourly precipitation data used in this study is more reliable than other observational and  
483 reanalysis precipitation data. In contrast with precipitation datasets, the observation of aerosols and clouds  
484 from MODIS might have larger uncertainties, e.g., which come from the misdetection of CF when AOD is  
485 large (Brennan et al., 2005; Levy et al., 2013) or the mutual interference between liquid and ice clouds (Holz  
486 et al., 2008; Platnick et al., 2017).

487 In this study we used two pollution indicators, AOD and CDNC, which discriminates the pollution levels  
488 for different purposes. AOD is a good proxy for the large-scale pollution level, but it stands for the optical  
489 feature of aerosols and cannot well represent CCN when we studied the aerosol-cloud interaction (Shinozuka  
490 et al., 2015). The value of AOD is also influenced by moisture condition, which is aerosol humidification  
491 effect (Twohy et al., 2009; Altaratz et al., 2013). Therefore, we comprehensively analyzed the moisture effect  
492 on the results. CDNC is a better proxy for CCN, which facilitates the study on the cloud changes associated  
493 with aerosol pollution. But the retrieved CDNC has larger uncertainties. First, the assumptions in the  
494 calculation of CDNC are idealized that CDNC is constant with height in a cloud and cloud liquid water  
495 increases monotonically at an adiabatic environment (Grosvenor et al., 2018). Second, as indicated by  
496 Grosvenor et al. (2018), the uncertainties in the pixel-level retrievals of CDNC from MODIS with  $1^\circ \times 1^\circ$   
497 spatial resolution can be above 54%, which come from the uncertainties of parameters and the original COD  
498 and CER data using in the calculation, and also the influence of heterogeneity effect from thin clouds. To  
499 reduce the influence of heterogeneity effect as much as possible, we have attempted to limit the conditions of  
500 CF, liquid COD and CER when calculating CDNC in the study. Besides, this study primarily applied the  
501 relative changes of CDNC, which actually reduced the uncertainties of absolute values.

502 We applied ultraviolet AI and AOD of BC/sulfate to identify different types of aerosols. The AI datasets  
503 from OMI, which can distinguish the absorbing aerosols and scattering aerosols, also have uncertainties  
504 especially for the near-zero values. Hence, we only compare the extreme circumstances of absorbing aerosols  
505 and scattering aerosols. We also found the AI has a weak positive correlation with AOD from MODIS, which  
506 indicates the results on absorbing aerosol days might represent the results on polluted days if identified by  
507 AOD. To avoid the uncertainty, we re-examined the results using AI when removing the polluted cases  
508 identified by AOD, and found the major results are not changed. The comparisons of BC/sulfate AOD cases  
509 also have uncertainties because they are retrieved from MACC reanalysis data. Although the above four  
510 indicators have their own uncertainties, currently we cannot find more reliable datasets in a long-term  
511 observational record, and the major findings can be well shown in these four indices.

512 Using AOD and CDNC we have drawn the same conclusion that the heavy rainfall occurs in advance and  
513 the duration is prolonged under pollution (Fig. 2). We found the AOD and CDNC only have a weak positive

514 correlation, which denotes that the selected cases could be different between using AOD and CDNC. The  
515 cases of heavy rainfall using CDNC seem more extreme, because CDNC cases exhibit more evident changes  
516 of rainfall behaviors in average than that using AOD. The difference of cases selected by the two indicators  
517 might due to the non-linear relationship of CCN and pollution that the CCN won't continuously increase when  
518 aerosol loading is huge (e.g., Jiang et al., 2016), or due to the misdetection of AOD and the calculation  
519 uncertainty of CDNC. Since both the two indicators have their uncertainties, we cannot say the result of which  
520 one is more reliable.

521 Most cloud properties also exhibit the consistent changes using CDNC and AOD. First, the CF, COT and  
522 CWP both for liquid and ice clouds increase with pollution, might because the aerosols serving as CCN can  
523 nucleate a larger number of cloud droplets and accumulate more liquid water in the cloud thus increase the CF,  
524 COT and CWP. Second, the CTP increases under pollution using both AOD and CDNC, which denotes the  
525 decrease of the cloud top height. We speculate that the earlier start of the precipitation process could inhibit  
526 the vertical growth of clouds shown as in Fig. 2. Third, the ice CER decreases under pollution using both  
527 AOD and CDNC, which could be ascribed to that the increased cloud droplet number leads to more cloud  
528 droplets transforming into ice crystals and causes the decrease of ice CER (Chylek et al., 2006; Zhao et al.,  
529 2018; Gryspeerdt et al., 2018). Currently the detailed physical processes of cold clouds and mixed-phase  
530 clouds are not clear, including the diffusional grow, accretion, riming and melting process of ice precipitation  
531 (Cheng et al., 2010), which needs numerical model simulations to be further explored.

532 However, the different result occurs for liquid CER between using AOD and using CDNC. The liquid CER  
533 is decreased when CDNC increases but increased when AOD increases (Fig. 7). The former is actually the  
534 natural result of the negative relationship between CDNC and liquid CER in the calculation. And the latter  
535 might be related to the aerosol humidification effect, the misdetection of AOD and cloud water, and also  
536 might result from the earlier formation of the clouds and heavy rainfall on the polluted days. Therefore, the  
537 changes of liquid CER with pollution have some uncertainties.

538

## 539 **7. Conclusions**

540 Using the gauge-based hourly rainfall records, aerosol and cloud satellite products and high temporal  
541 resolution reanalysis datasets during 2002-2012, this study investigated the different characteristics of heavy  
542 rainfall in the diurnal time scale on the clean and polluted conditions respectively. Based on two indicators  
543 that are AOD from MODIS aerosol product and retrieved CDNC from MODIS cloud product, we found three  
544 features of rainfall changing by aerosols that the rainfall start and peak time occur earlier and the duration  
545 becomes longer. The quantitative differences exist between the two indicators, i.e., the statistic differences of  
546 above features between clean and polluted conditions are 0.7, 1.0, 0.8 hours based on AOD and 1.4, 3.0, 2.2  
547 hours based on CDNC. The different roles of absorbing aerosols and scattering aerosols in modifying the



548 diurnal shift were also distinguishable using ultraviolet AI from OMI and reanalysis AOD of two aerosol types  
549 (BC and sulfate). The absorbing aerosols (BC) correspond to the earlier start time and peak time of heavy  
550 rainfall, while the scattering aerosols (sulfate) correspond to the delayed start time and the longer duration. To  
551 distinguish the influence of aerosols, the influence of moisture (SH at 850 hPa) on the heavy rainfall is also  
552 investigated, which shows similar with the scattering aerosols (sulfate). By comparing the characteristics of  
553 cloud macrophysics and microphysics variables, using both AOD and CDNC we found the CF, COT (liquid  
554 and ice), CWP (liquid and ice) are increased on the polluted condition, but the cloud top height and the ice  
555 CER are reduced. Comparing the influence of CCN and moisture respectively on these cloud variables, the  
556 cloud properties show similar changes with the increase of CCN and moisture, but seem more sensitive to the  
557 CCN.

558 According to these results, we speculate that both aerosol radiative effect and cloud effect have impacts on  
559 the diurnal variation of heavy rainfall in the BTH region. The heating effect of absorbing aerosols especially  
560 BC increases the instability of the lower to middle atmosphere so that generates the heavy rainfall occurrence  
561 in advance. And the increased moisture supply and increased aerosols which nucleate more cloud droplets and  
562 accumulate more liquid water in clouds, lead to the longer duration of heavy rainfall.

563 This study has clearly identified the aerosol effect on diurnal changes of heavy rainfall and concurrent  
564 clouds in the BTH region and attempted to address the causes. However, although this work has attempted to  
565 exclude the impacts from the meteorological background particularly circulation and moisture, the observation  
566 study still has its limitation on studying aerosol effect on rainfall and cloud, such as the noise and uncertainty  
567 of different observational data, the interaction of aerosol and meteorological factors and the mixing of  
568 different types of aerosols. Numerical model simulations are necessarily applied to examine the speculation  
569 we proposed here. And the specific processes of aerosols effect on the mix-phased cloud precipitation  
570 formation also needs further exploration in our future study.

571

## 572 **Data availability**

573 We are grateful to the National Meteorological Information Centre (NMIC) of the China Meteorological  
574 Administration (CMA) for providing hourly precipitation datasets. MODIS aerosol and cloud data were  
575 obtained from <http://ladsweb.modaps.eosdis.nasa.gov>; ultraviolet AI data from OMI was obtained from  
576 <https://daac.gsfc.nasa.gov/datasets?keywords=OMI&page=1>; MACC-II and ERA-interim reanalysis datasets  
577 were obtained from <http://apps.ecmwf.int/datasets>.

## 578 **Author contributions**

579 JY and SZ conceived the study. SZ processed data and drew the figures. SZ and JY analyzed the observational  
580 results and WCW, CZ and DG gave the professional guidance. PS provided the hourly precipitation dataset.  
581 SZ and JY prepared the manuscript with contributions from WCW and CZ.

582 **Competing interests**

583 The authors declare that they have no conflict of interest.

584 **Acknowledgements**

585 This study is supported by funds from the National Key Research and Development Program-Global Change  
586 and Mitigation Project: Global Change Risk of Population and Economic System: Mechanism and Assessment  
587 (2016YFA0602401), the National Natural Science Foundation of China (grant nos. 41375003, 41621061 and  
588 41575143) and Project supported by State Key Laboratory of Earth Surface Processes and Resource Ecology  
589 and Key Laboratory of Environmental Change and Natural Disaster. Wei-Chyung Wang acknowledges the  
590 support of a grant (to SUNYA) from the Office of Sciences (BER), U.S. DOE.

591

592 **References:**

- 593 Albrecht, B. A.: Aerosols, cloud microphysics, and fractional cloudiness, *Science* 245: 1227-1230, 1989.
- 594 Altaratz, O., Bar-Or, R. Z., Wollner, U., and Koren, I.: Relative humidity and its effect on aerosol optical  
595 depth in the vicinity of convective clouds, *Environ. Res. Lett.*, 8, 034025, 2013.
- 596 Anonymous: 1994. *Atmospheric Sciences Thesaurus*. China Meteorological Press: Beijing, China. (in  
597 Chinese)
- 598 Anonymous (2013), IPCC fifth assessment report, *Weather*, 68, 310-310.
- 599 Bellouin, N., Quaas, J., Morcrette J. -J., and Boucher, O.: Estimates of aerosol radiative forcing from the  
600 MACC re-analysis. *Atmos. Chem. Phys.*, 13: 2045-2062, 2013.
- 601 Benedetti, A., Morcrette, J. J., Boucher, O., Dethof, A., Engelen, R. J., Fisher, M., Flentje, H., Huneeus, N.,  
602 Jones, L., Kaiser, J. W., Kinne, S., Mangold, A., Razinger, M., Simmons, A. J., and Suttie, M.: Aerosol  
603 analysis and forecast in the European Centre for Medium-Range Weather Forecasts Integrated Forecast  
604 System: 2. Data assimilation. *J. Geophys. Res.* 114: D13205 doi:10.1029/2008JD011115, 2009.
- 605 Brennan, J., Kaufman, Y., Koren, I., and Rong, L.: Aerosol-cloud interaction-Misclassification of MODIS  
606 clouds in heavy aerosol, *IEEE T. Geosci. Remote*, 43, 911-915,  
607 <https://doi.org/10.1109/TGRS.2005.844662>, 2005.
- 608 Bennartz, R., and Rausch, J.: Global and regional estimates of warm cloud droplet number concentration  
609 based on 13 years of AQUA-MODIS observations, *Atmos. Chem. Phys.*, 17: 9815-9836, 2017.
- 610 Bennartz, R.: Global assessment of marine boundary layer cloud droplet number concentration from satellite, *J.*  
611 *Geophys. Res.*, 112, D02201, doi:10.1029/2006JD007547, 2007.
- 612 Boers, R., Acarreta, J. A., and Gras, J. L.: Satellite monitoring of the first indirect aerosol effect: Retrieval of  
613 the droplet concentration of water clouds, *J. Geophys. Res.*, 111, D22208, doi:10.1029/2005JD006838,  
614 2006.
- 615 Chen, Q., Yin, Y., Jin, L., Xiao, H., and Zhu, S.: The effect of aerosol layers on convective cloud  
616 microphysics and precipitation, *Atmos. Res.*, **101**, 327-340, 2011.

617 Cheng, C. T., Wang, W. C., and Chen, J. P.: A modeling study of aerosol impacts on cloud microphysics and  
618 radiative properties, *Q. J. R. Meteorol. Soc.*, 133, 283–297, doi:10.1002/qj.25, 2007.

619 Cheng, C. T., Wang, W. C., and Chen, J. P.: Simulation of the effects of increasing cloud condensation nuclei  
620 on mixed-phase clouds and precipitation of a front system. *Atmos. Res.*, 96: 461-476, doi:  
621 10.1016/j.atmosres.2010.02.005, 2010.

622 Chylek, P., Dubey, M. K., Lohmann, U., Ramanathan, V., Kaufman, Y. J., Lesins, G., Hudson, J., Altmann,  
623 G., and Olsen, S.: Aerosol indirect effect over the Indian Ocean, *Geophys. Res. Lett.*, 33(6), L06806,  
624 doi:10.1029/2005GL025397, 2006.

625 Dee, D. P., Uppala, S. M., Simmons, A. J., Berrisford, P., Poli, P., Kobayashi, S., Andrae, U., Balmaseda, M.  
626 A., Balsamo, G., Bauer, P., Bechtold, P., Beljaars, A. C. M., van de Berg, L., Bidlot, J., Bormann, N.,  
627 Delsol, C., Dragani, R., Fuentes, M., Geer, A. J., Haimberger, L., Healy, S. B., Hersbach, H., Hólm, E.  
628 V., Isaksen, I., Kallberg, P., Köhler, M., Matricardi, M., McNally, A. P., Monge-Sanz, B. M.,  
629 Morcrette, J.-J., Park, B.-K., Peubey, C., de Rosnay, P., Tavolato, C., Thépaut, J.-N., Vitart, F.: The  
630 ERA-Interim reanalysis: configuration and performance of the data assimilation system. *Q. J. R.*  
631 *Meteorol. Soc.* 137: 553–597. doi:10.1002/qj.828, 2011.

632 Fan, J. W., Rosenfeld, D., Yang, Y., Zhao, C., Leung, L. R., and Li, Z. Q.: Substantial contribution of  
633 anthropogenic air pollution to catastrophic floods in Southwest China. *Geophys. Res. Lett.* 42:  
634 6066-6075, 2015.

635 Garrett, T. J. and Zhao, C.: Increased Arctic cloud longwave emissivity associated with pollution from  
636 mid-latitudes. *Nature* 440(7085): 787-9, 2006.

637 Givati, A., and Rosenfeld, D.: Quantifying precipitation suppression due to air pollution. *J. Appl. Meteor.* 43:  
638 1038-1056, 2004.

639 Grandey, B. S., and Stier, P.: A critical look at spatial scale choices in satellite-based aerosol indirect effect  
640 studies, *Atmos. Chem. Phys.*, 10(23), 11459–11470, doi:10.5194/acp-10-11459-2010, 2010.

641 Gryspeerdt, E., Sourdeval, O., Quaas, J., Delanoë, J., Krämer, M., and Kühne, P.: Ice crystal number  
642 concentration estimates from lidar–radar satellite remote sensing – Part 2: Controls on the ice crystal  
643 number concentration, *Atmos. Chem. Phys.*, 18(19), 14351–14370, doi:10.5194/acp-18-14351-2018,  
644 2018.

645 Gryspeerdt, E., Stier, P., and Partridge, D. G.: Links between satellite-retrieved aerosol and precipitation.  
646 *Atmos. Chem. Phys.*, 14, 9677–9694, 2014.

647 Gunthe, S. S., Rose, D., Su, H., Garland, R. M., Achtert, P., Nowak, A., Wiedensohler, A., Kuwata, M.,  
648 Takegawa, N., Kondo, Y., Hu, M., Shao, M., Zhu, T., Andreae, M. O., and Poschl, U.: Cloud  
649 condensation nuclei (CCN) from fresh and aged air pollution in the megacity region of Beijing, *Atmos.*  
650 *Chem. Phys.* 11(21): 11023-11039, 2011.

651 Guo, C. W., Xiao, H., Yang, H. L., and Tang, Q.: Observation and modeling analyses of the macro-and  
652 microphysical characteristics of a heavy rain storm in Beijing, *Atmos. Res.*, 156: 125-141, doi:

653 10.1016/j.atmosres.2015.01.007, 2015.

654 Guo, J. P., Deng, M. J., Lee, S. S., Wang, F., Li, Z. Q., Zhai, P. M., Liu, H., Lv, W., Yao, W., and Li, X. W.:  
655 Delaying precipitation and lightning by air pollution over the Pearl River Delta. Part I: Observational  
656 analyses. *J. Geophys. Res. Atmos.* 121: 6472-6488, 2016.

657 Guo, L., Highwood, E. J., Shaffrey, L. C., and Turner, A. G.: The effect of regional changes in anthropogenic  
658 aerosols on rainfall of the East Asian Summer Monsoon. *Atmos. Chem. Phys.* 13: 1521-1534, 2013.

659 Guo, X. L., Fu, D. H., Guo, X., and Zhang, C. M.: A case study of aerosol impacts on summer convective  
660 clouds and precipitation over northern China. *Atmos. Res.* 142: 142-157, 2014.

661 Hammer, M. S., Martin, R. V., Li, C., Torres, O., Manning, M., and Boys, B. L.: Insight into global trends in  
662 aerosol composition from 2005 to 2015 inferred from the OMI Ultraviolet Aerosol Index, *Atmos. Chem.*  
663 *Phys.*, 18: 8097-8112, 2018.

664 Harikishan, G., Padmakumari, B., Maheskumar, R. S., Pandithurai, G., and Min, Q. L.: Aerosol indirect effects  
665 from ground-based retrievals over the rain shadow region in Indian subcontinent, *J. Geophys. Res. Atmos.*  
666 121(5): 2369-2382, 2016.

667 Higgins, R. W., Yao, Y., Yarosh, E. S., Janowiak, J. E. and Mo, K. C.: Influence of the Great Plains low-level  
668 jet on summertime precipitation and moisture transport over the central United States, *J. Climate*, 10,  
669 481-507, 1997.

670 Holz, R. E., Ackerman, S. A., Nagle, F. W., Frey, R., Dutcher, S., Kuehn, R. E., Vaughan, M. A., and Baum,  
671 B.: Global Moderate Resolution Imaging Spectroradiometer (MODIS) cloud detection and height  
672 evaluation using CALIOP, *J. Geophys. Res. Atmos.*, 113: D00A19, doi: 10.1029/2008JD009837, 2008.

673 Jacobson, M. Z.: Strong radiative heating due to the mixing state of black carbon in atmospheric aerosols.  
674 *Nature* 409: 695-697, 2001.

675 Jiang, H., Feingold, G., and Cotton, W. R.: Simulations of aerosol-cloud-dynamical feedbacks resulting from  
676 entrainment of aerosol into the marine boundary layer during the Atlantic Stratocumulus Transition  
677 Experiment, *J. Geophys. Res.*, 107(D24), 4813, doi:10.1029/2001JD001502, 2002.

678 Jiang, J. H., Su, H., Schoeberl, M. R., Massie, S. T., Colarco, P., Platnick, S., and Livesey, N. J.: Clean and  
679 polluted clouds: Relationships among pollution, ice clouds, and precipitation in South America, *Geophys.*  
680 *Res. Lett.*, 35, L14804, doi: 10.1029/2008GL034631, 2008.

681 Jiang, M. J., Li, Z. Q., Wan, B. C., and Cribb, M.: Impact of aerosols on precipitation from deep convective  
682 clouds in eastern China. *J. Geophys. Res.* 121: 9607-9620, 2016.

683 Johnson, D. B.: The role of giant and ultra-giant aerosol particles in warm rain initiation, *J. Atmos. Sci.*, 39,  
684 448-460, doi:10.1175/1520-0469(1982)039<0448:TROGAU>2.0.CO;2, 1982.

685 Jung, W. S., Panicker, A. S., Lee, D. I., and Park, S. H.: Estimates of aerosol indirect effect from Terra  
686 MODIS over Republic of Korea, *Advances in Meteorology*, 2013 (976813): 1-8,  
687 <http://dx.doi.org/10.1155/2013/976813>, 2013.

688 Kim, K. -M., Lau, K. M., Sud, Y. C., and Walker, G. K.: Influence of aerosol radiative forcings on the diurnal  
689 and seasonal cycles of rainfall over West Africa and Eastern Atlantic Ocean using GCM simulation. *Clim.*  
690 *Dyn.* 35(1):115-126, doi: 10.1007/s00382-010-0750-1, 2010.

691 Lau, K. M., Kim, M. K., and Kim, K. M.: Asian summer monsoon anomalies induced by aerosol direct  
692 forcing: the role of the Tibetan Plateau. *Clim. Dyn.*, 26: 855-864, 2006.

693 Lee, S. S., Donner, L. J., and Phillips, V. T. J.: Impacts of aerosol chemical composition on microphysics and  
694 precipitation in deep convection. *Atmos. Res.*, 94, 220-237, 2009.

695 Lee, S. S., Guo, J., and Li, Z: Delaying precipitation by air pollution over the Pearl River Delta: 2. Model  
696 simulation. *J. Geophys. Res. Atmos.*, 121: 11739-11760, 2016.

697 Lelieveld, J. and Heintzenberg, J.: Sulfate cooling effect on climate through in-cloud oxidation of  
698 anthropogenic SO<sub>2</sub>. *Science* 258: 117-120, 1992.

699 Levy, R. C., Mattoo, S., Munchak, L. A., Remer, L. A., Sayer, A. M., Patadia, F., and Hsu, N. C.: The  
700 Collection 6 MODIS aerosol products over land and ocean, *Atmos. Meas. Tech.*, 6, 2989–3034,  
701 <https://doi.org/10.5194/amt-6-2989-2013>, 2013.

702 Li, H., Cui, X., Zhang, W., and Qiao, L.: Observational and dynamic downscaling analysis of a heavy rainfall  
703 event in Beijing, China during the 2008 Olympic Games, *Atmos. Sci. Lett.*, 17, 368-376, 2016.

704 Li, Z., Niu, F., Fan, J., Liu, Y., Rosenfeld, D., and Ding, Y.: Long-term impacts of aerosols on the vertical  
705 development of clouds and precipitation, *Nat. Geosci.*, 4, 888-894, 2011.

706 Lim, K. S. and Hong, S.: Investigation of aerosol indirect effects on simulated flash-flood heavy rainfall over  
707 Korea, *Meteor. Atmos. Phys.*, **118**, 199-214, 2012.

708 Liu, G., Shao, H., Coakley Jr. J. A., Curry, J. A., Haggerty, J. A., and Tschudi, M. A.: Retrieval of cloud  
709 droplet size from visible and microwave radiometric measurements during INDOEX: Implication to  
710 aerosols' indirect radioactive effect, *J. Geophys. Res.*, 108(D1), 4006, doi:10.1029/2001JD001395, 2003.

711 Liu, J., Wang, S., Zhang, W., and Wei, X.: Mechanism analysis of a strong convective weather in Hebei  
712 Province, *Advances in Marine Science*, 30, 9-16, 2012.

713 Menzel, W. P., Frey, R. A., Zhang, H., Wylie, D. P., Moeller, C. C., Holz, R. E., Maddux, B., Baum, B. A.,  
714 Strabala, K. I., and Gumley, L. E.: MODIS global cloud-top pressure and amount estimation: Algorithm  
715 description and results, *J. Appl. Meteorol. Clim.*, 47(4):1175-1198, doi: 10.1175/2007JAMC1705.1,  
716 2008.

717 Min, Q., Joseph, E., Lin, Y., Min, L., Yin, B., Daum, P. H., Kleinman, L. I., Wang, J., and Lee, Y. -N.:  
718 Comparison of MODIS cloud microphysical properties with in-situ measurements over the Southeast  
719 Pacific, *Atmos. Chem. Phys.*, 12: 11261-11273, 2012.

720 Nakajima, T. and King, M. D.: Determination of the optical thickness and effective particle radius of clouds  
721 from reflected solar radiation measurements. Part I: Theory, *J. Atmos. Sci.*, 47, 1878-1893, 1990.

722 Panicker, A. S., Pandithurai, G., and Dipu, S.: Aerosol indirect effect during successive contrasting monsoon  
723 seasons over Indian subcontinent using MODIS data, *Atmospheric environment* 44(15): 1937-1943,  
724 2010.

725 Platnick, S., Meyer, K., King, M. D., Wind, G., Amarasinghe, N., Marchant, B., Arnold, G. T., Zhang, Z.,  
726 Hubanks, P. A., Holz, R. E., Yang, P., Ridgway, W. L., and Riedi, J.: The MODIS cloud optical and

727 microphysical products: Collection 6 updates and examples from Terra and Aqua. *IEEE Trans. Geosci.*  
728 *Remote Sens.*, 55, 502-525, doi:10.1109/TGRS.2016.2610522, 2017

729 Qian, Y., Gong, D. Y., Fan, J. W., Leung, L. R., Bennartz, R., Chen, D. L., Wang, W. G.: Heavy pollution  
730 suppresses light rain in China: Observations and modeling. *J. Geophys. Res. Atmos.* **114**: D00K02, 2009.

731 Qiu, Y., Zhao, C., Guo, J., and Li, J.: 8-Year ground-based observational analysis about the seasonal variation  
732 of the aerosol-cloud droplet effective radius relationship at SGP site. *Atmos. Environ.* 164: 139-146,  
733 2017.

734 Quaas, J., Boucher, O., Bellouin, N. and Kinne, S.: Satellite-based estimate of the direct and indirect aerosol  
735 climate forcing, *J. Geophys. Res.*, 113, D05204, doi:10.1029/2007JD008962, 2008.

736 Rienecker, M. M., Suarez, M. J., Todling, R., Bacmeister, J., Takacs, L., Liu, H. C., Gu, W., Sienkiewicz, M.,  
737 Koster, R. D., Gelaro, R., Stajner, I., Nielsen, J. E.: The GEOS-5 Data Assimilation  
738 System—Documentation of Versions 5.0.1 and 5.1.0, and 5.2.0. NASA Technical Report Series on  
739 Global Modeling and Data Assimilation NASA/TM-2008 -104606 27: 92 pp, 2008.

740 Rosenfeld, D.: TRMM observed first direct evidence of smoke from forest fires inhibiting rainfall, *Geophys.*  
741 *Res. Lett.*, 26, 3105–3108, doi:10.1029/1999GL006066, 1999.

742 Rosenfeld, D., Lohmann, U., Raga, G. B., O'Dowd, C. D., Kulmala, M., Fuzzi, S., Reissell, A., Andreae, M.  
743 O.: Flood or drought: How do aerosols affect precipitation? *Science*, 321:1309-1313, 2008.

744 Rosenfeld, D., Sherwood, S., Wood, R., and Donner, L.: Climate effects of aerosol-cloud interactions. *Science*,  
745 343: 379-380, 2014.

746 Rosenfeld, D., and Woodley, W. L.: Convective clouds with sustained highly supercooled liquid water down  
747 to  $-37^{\circ}\text{C}$ , *Nature*, 405, 440–442, doi:10.1038/35013030, 2000.

748 Sassen, K., Starr, D., Mace, G. G., Poellot, M. R., Melfi, S. H., Eberhard, W.L., Spinhirne, J. D., Eloranta, E.  
749 W., Hagan, D. E., and Hallett, J.: The 5–6 December 1991 FIRE IFO II jet stream cirrus case study:  
750 Possible influences of volcanic aerosols, *J. Atmos. Sci.*, 52, 97–123, doi:10.1175/1520-0469(1995)  
751 052<0097:TDFIJJ>2.0.CO;2, 1995.

752 Shen, Y., Xiong, A., Wang, Y., and Xie, P.: Performance of high-resolution satellite precipitation products  
753 over China, *J. Geophys. Res.*, 115, D02114, doi:10.1029/2009JD012097, 2010.

754 Sherwood, S.: Aerosols and ice particle size in tropical cumulonimbus, *J. Clim.*, 15, 1051–1063,  
755 doi:10.1175/1520-0442(2002)015<1051:AAIPSI>2.0.CO;2, 2002.

756 Shinozuka, Y., Clarke, A. D., Nenes, A., Jefferson, A., Wood, R., McNaughton, C. S., Ström, J., Tunved, P.,  
757 Redemann, J., Thornhill, K. L., Moore, R. H., Latham, T. L., Lin, J. J., and Yoon, Y. J.: The relationship  
758 between cloud condensation nuclei (CCN) concentration and light extinction of dried particles:  
759 indications of underlying aerosol processes and implications for satellite-based CCN estimates, *Atmos.*  
760 *Chem. Phys.*, 15, 7585-7604, 10.5194/acp-15-7585-2015, 2015.

761 Song, X. L. and Zhang, G. J.: Microphysics parameterization for connective clouds in a global climate model:  
762 Description and single-column model tests, *J. Geophys. Res. Atmos.*, 116, D02201, 2011.

763 Squires, P.: The growth of cloud drops by condensation: I. general characteristics, *Aust. J. Sci. Res., Ser. A*, 5,  
764 66–86, 1952.

765 Squires, P., and Twomey, S.: A comparison of cloud nucleus measurements over central North America and  
766 Caribbean Sea, *J. Atmos. Sci.*, 23, 401–404, doi: 10.1175/1520-0469(1966)023<0401:ACOCNM>  
767 -2.0.CO;2, 1966.

768 Sun, Y. L., Wang, Z. F., Du, W., Zhang, Q., Wang, Q. Q., Fu, P. Q., Pan, X. L., Li, J., Jayne, J., and Worsnop,  
769 D. R.: Long-term real-time measurements of aerosol particle composition in Beijing, China: seasonal  
770 variations, meteorological effects, and source analysis, *Atmos. Chem. Phys.*, 15: 10149-10165, 2015.

771 Tariq, S., and Ali, M.: Spatio-temporal distribution of absorbing aerosols over Pakistan retrieved from OMI on  
772 board Aura Satellite. *Atmos. Pollution Res.* doi: 10.5094/APR.2015.030, 2015.

773 Tao, M. H., Chen, L. F., Wang, Z. F., Tao, J. H., Che, H. Z., Wang, X. H., and Wang, Y.: Comparison and  
774 evaluation of the MODIS Collection 6 aerosol data in China. *J. Geophys. Res. Atmos.* 120:6992-7005,  
775 2015.

776 Tao, W. K., Chen, J. P., Li, Z., Wang, C., and Zhang C.: Impact of aerosols on convective clouds and  
777 precipitation. *Rev. Geophys.*, 50, RG2001/2012: 1-62, doi: 10.1029/2011RG000369, 2012.

778 Torres, O., Bhartia, P.K., Herman, J.R., Ahmad, Z., Gleason, J.: Derivation of aerosol properties from satellite  
779 measurements of backscattered ultraviolet radiation: Theoretical basis. *J. Geophys. Res. Atmos.* 103:  
780 17099–17110, 1998.

781 Twohy, C. H., Coakley, J. A., and Tahnk, W. R.: Effect of changes in relative humidity on aerosol scattering  
782 near clouds, *Journal of Geophysical Research: Atmospheres*, 114, n/a-n/a, 10.1029/2008JD010991, 2009.

783 Twomey, S.: The influence of pollution on the shortwave albedo of clouds, *J. Atmos. Sci.*, 34, 1149–1152,  
784 doi:10.1175/1520-0469(1977)034<1149:TIOPOT>2.0.CO;2, 1977.

785 Wang, J., Feng, J., Wu, Q., and Z. Yan, Z.: Impact of anthropogenic aerosols on summer precipitation in the  
786 Beijing-Tianjin-Hebei urban agglomeration in China: Regional climate modeling using WRF-Chem. *Adv.*  
787 *Atmos. Sci.*, **33**, 753-766, 2016.

788 Wang, Z., Guo, P., and Zhang, H.: A Numerical Study of Direct Radiative Forcing Due to Black Carbon and  
789 Its Effects on the Summer Precipitation in China. *Climatic and Environmental Research*, **14**, 161-171,  
790 2009.

791 Wolyn, P. G., and Mckee, T. B.: The mountain plains circulation east of a 2-km-high north south barrier, *Mon.*  
792 *Weather Rev.*, 122, 1490-1508, 1994.

793 Wu, P., Ding, Y. H., and Liu, Y. J.: Atmospheric circulation and dynamic mechanism for persistent haze  
794 events in the Beijing-Tianjin-Hebei region, *Adv. Atmos. Sci.*, 34(4): 429-440, 2017.

795 Yang, X., Zhao, C., Zhou, L., Li, Z., Cribb, M., and Yang, S.: Wintertime cooling and a potential connection  
796 with transported aerosols in Hong Kong during recent decades. *Atmos. Res.* 211: 52-61, 2018.

797 Yu, R. C., Zhou, T. J., Xiong, A. Y., Zhu, Y. J., and Li, J. M.: Diurnal variations of summer precipitation over  
798 contiguous China. *Geophys. Res. Lett.* 34: L017041, 2007.

799 Yuan, T., Li, Z., Zhang, R., and Fan, J.: Increase of cloud droplet size with aerosol optical depth: An

800 observation and modeling study. *J. Geophys. Res. Atmos.*, 113: D04201, 2008.

801 Yuan, W. H., Yu, R. C., Chen, H. M., Li, J., and Zhang, M. H.: Subseasonal Characteristics of Diurnal  
802 Variation in Summer Monsoon Rainfall over Central Eastern China. *J. Climate* 23:6684-6695, 2010.

803 Zeng, S., Riedi, J., Trepte, C. R., Winker, D. M., and Hu, Y. -X.: Study of global cloud droplet number  
804 concentration with A-Train satellites. *Atmos. Chem. Phys.*, 14: 7125-7134, doi:  
805 10.5194/acp-14-7125-2014, 2014.

806 Zhao, B., Gu, Y., Liou, K. -N., Wang, Y., Liu, X., Huang, L., Jiang, J. H., and Su, H.: Type-Dependent  
807 Responses of Ice Cloud Properties to Aerosols From Satellite Retrievals, *Geophys. Res. Lett.*, 45(7),  
808 3297–3306, doi:10.1002/2018GL077261, 2018.

809 Zhou, S., Yang, J., Wang, W. C., Gong, D., Shi, P., and Gao, M.: Shift of daily rainfall peaks over the  
810 Beijing– Tianjin– Hebei region: An indication of pollutant effects? *Int. J. Climatol.* 2018:1–10.  
811 <https://doi.org/10.1002/joc.5700>, 2018.

812 Zhu, Y., Rosenfeld, D., and Li, Z.: Under what conditions can we trust retrieved cloud drop concentrations in  
813 broken marine stratocumulus? *J. Geophys. Res. Atmos.*, 123: 8754-8767, 2018.

814

815

816

817

818

819

820

821

822

823

824

825

826

827

828

829

830

831

832

833

834

835



836 **Tables**

837

838

Indicator	Data from	Time	Clean/less (< 25th)	Polluted/more (>75th)
AOD	MODIS	2002-2012	0.98	2.00
CDNC (cm <sup>-3</sup> )	MODIS	2002-2012	952.06	2878.58
AAI	OMI	2005-2012	0.13	0.52
SAI	OMI	2005-2012	- 0.13	- 0.35
BC AOD	MACC	2003-2012	0.04	0.06
Sulfate AOD	MACC	2003-2012	0.46	0.87
SH at 850 hPa (g/kg)	ERA-interim	2002-2012	9.96	12.95

839

840 Table 1. The indicators used in the study and their thresholds for clean/less and polluted/more conditions.

841

842

843

844

845

Characteristics of heavy rainfall	Average of clean condition		Average of polluted condition		Difference (polluted - clean)		Significance of difference	
	AOD	CDNC	AOD	CDNC	AOD	CDNC	AOD	CDNC
Start time (LST)	24.2	24.3	23.5	22.9	- 0.7	- 1.4	P<0.05	P<0.05
Peak time (LST)	23.0	22.1	22.0	19.1	- 1.0	- 3.0	P<0.05	P<0.05
Duration (hours)	4.0	5.5	4.8	7.7	+ 0.8	+ 2.2	P<0.05	P<0.05
Intensity (0.1mm/hour)	164.9	166.0	169.6	162.7	+ 4.7	- 3.3	P>0.1	P>0.1

846

847 Table 2. The average values of start time (units: LST), peak time (units: LST), duration (units: hours) and  
 848 intensity (units: 0.1mm/hour) of heavy rainfall respectively on the clean and polluted conditions using two  
 849 indicators of AOD and CDNC, and the differences and significances between clean and polluted conditions.  
 850 “P<0.05” stands for the difference has passed the significance test of 95%, and “P>0.1” stands for the  
 851 difference did not pass the significance test of 90%.

852

Characteristics of heavy rainfall	AAI	SAI	Difference (A-S)	Less BC	More BC	Difference (M-L)	Less sulfate	More sulfate	Difference (M-L)
Start time (LST)	23.4	24.1	-0.7 P<0.05	24.2	23.9	-0.3 P<0.05	24.0	24.5	0.5 P<0.05
Peak time (LST)	21.0	22.6	-1.6 P<0.05	23.4	22.3	-1.1 P<0.05	23.2	22.9	-0.3 P<0.05
Duration (hours)	5.0	6.0	-1.0 P<0.05	4.8	4.6	-0.2 P<0.05	4.0	5.5	1.5 P<0.05

854

855 Table 3. The average values of start time (units: LST), peak time (units: LST) and duration (units: hours) of  
856 heavy rainfall respectively on the conditions with absorbing aerosols, scattering aerosols, less BC, more BC,  
857 less sulfate and more sulfate, and their differences and significances.

858

859

Clean/Polluted	CF	CTP	COT (liquid)	COT (ice)	CWP (liquid)	CWP (ice)	CER (liquid)	CER (ice)
Clean (AOD)	62.8	442.3	6.9	6.7	62.8	123.1	16.7	32.0
Polluted (AOD)	89.3	487.3	10.0	12.9	96.4	211.3	17.5	29.2
Difference [P - C]	26.5	45.0	3.1	6.2	33.6	88.2	0.8	-2.8
Percentage [(P-C)/C]	42.2%	10.2%	44.9%	92.5%	53.5%	71.6%	4.8%	-8.8%
Clean (CDNC)	94.5	398.0	8.1	8.7	102.4	171.6	20.4	34.2
Polluted (CDNC)	97.4	430.8	40.4	33.1	318.2	542.5	12.2	25.4
Difference [P - C]	2.9	32.8	32.3	24.4	216.0	371.0	-8.2	-8.8
Percentage [(P-C)/C]	3.1%	8.2%	398.8%	280.5%	210.7%	216.1%	-40.2%	-25.7%

860

861 Table 4. The average values of CF (units: %), CTP (units: hPa), COT (liquid and ice, units: none), CWP  
862 (liquid and ice, units: g/m<sup>2</sup>) and CER (liquid and ice, units: μm) on clean condition and polluted conditions  
863 using two indicators of AOD and CDNC, and their differences (polluted minus clean) and percentages. The  
864 differences have all passed the significant test of 95%.

865

866

867

868

Group (case number)	CF	CTP	COT (liquid)	COT (ice)	CWP (liquid)	CWP (ice)	CER (liquid)	CER (ice)
1.Clean, dry (153)	93.8	393.3	7.2	7.6	88.7	149.0	20.4	36.7
2.Polluted, dry (128)	95.6	475.7	50.2	43.4	424.6	793.5	12.6	30.0
3.Clean, wet (155)	92.7 <small>0.05&lt;p<sub>1,3</sub>&lt;0.1</small>	457.4	8.6	10.6	101.9	207.7	19.8 <small>0.05&lt;p<sub>1,3</sub>&lt;0.1</small>	33.2
4.Polluted, wet (194)	97.8	419.7 <small>0.05&lt;p<sub>3,4</sub>&lt;0.1</small>	36.4	28.4	295.9	456.4	12.5 <small>p<sub>2,4</sub>&gt;0.1</small>	24.4

869

870 Table 5. The average values of CF (units: %), CTP (units: hPa), COT (liquid and ice, units: none), CWP  
871 (liquid and ice, units: g/m<sup>2</sup>) and CER (liquid and ice, units: μm) in four groups. Grey numbers represent that  
872 the differences are not significant, in which “0.05<P<0.1” stands for the difference has passed the significance  
873 test of 90% but did not pass the significance test of 95%, and “P>0.1” stands for the difference did not pass  
874 the significance test of 90%.

875

876

877

878

879

880

881

882

883

884

885

886

887

888

889

890

891

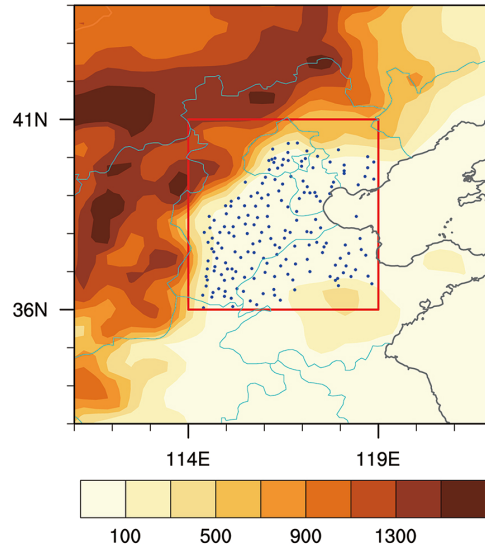
892

893

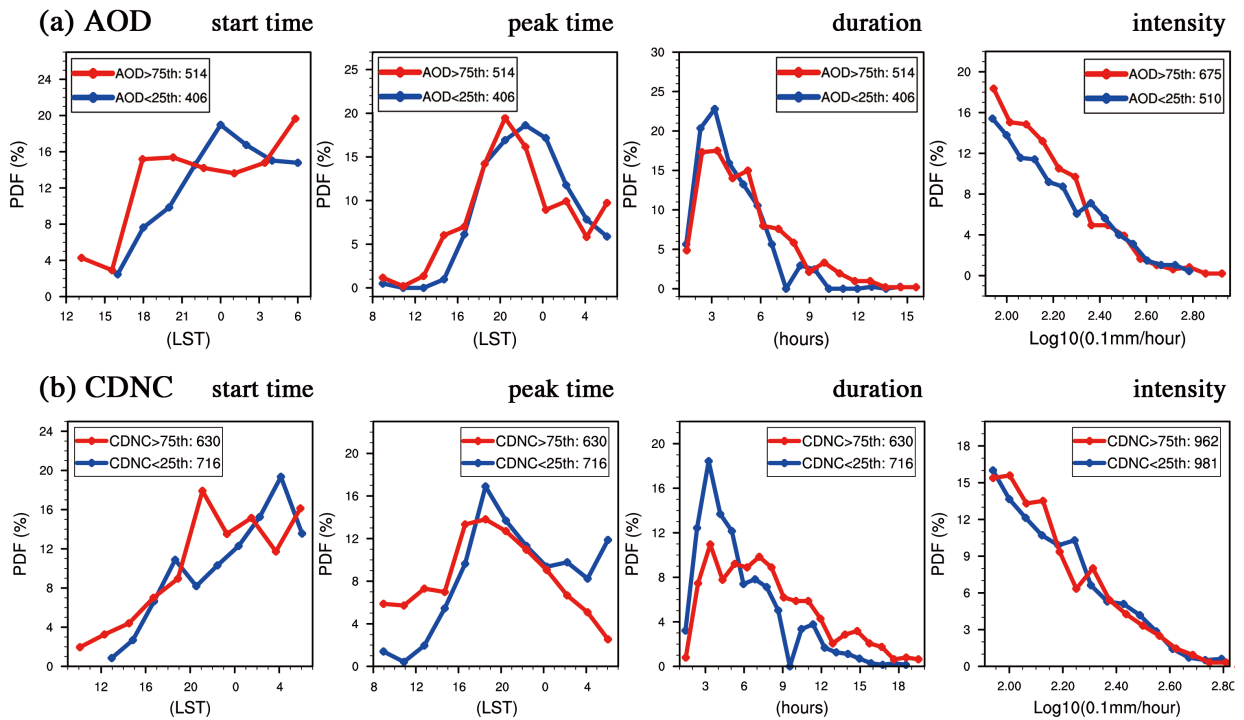
894

895

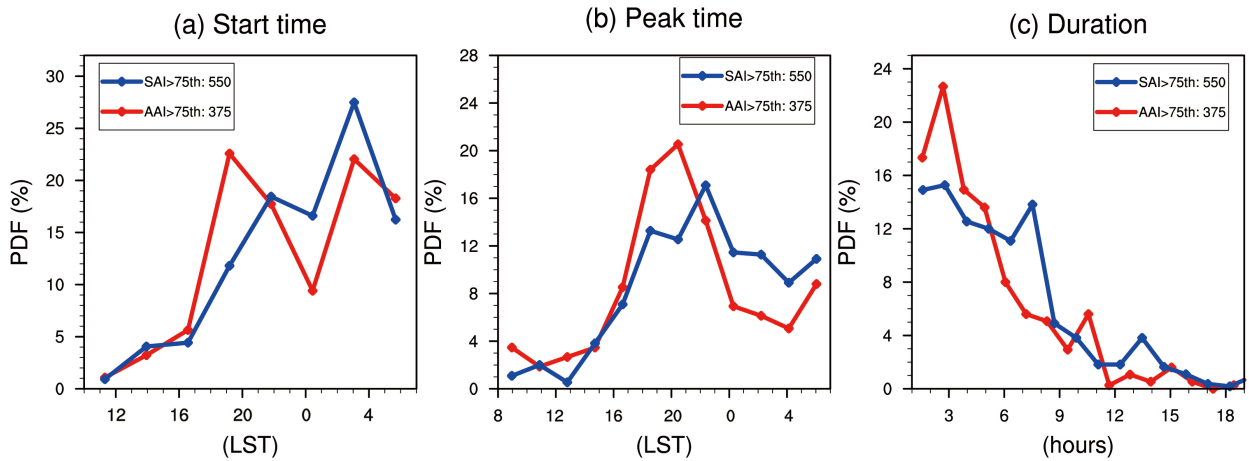
896



900 Figure 1. Altitudes (shading, units: m) and selected stations (dots) in the BTH region (red box, 36–41° N,  
901 114–119° E).



905 Figure 2. PDF of start time (units: LST), peak time (units: LST), duration (units: hours) and intensity (units:  
906 0.1mm/hour) of heavy rainfall on selected clean (blue lines) and polluted (red lines) conditions, respectively  
907 using indicator of (a) AOD and (b) CDNC (cm<sup>-3</sup>), during early summers from 2002 to 2012.



909

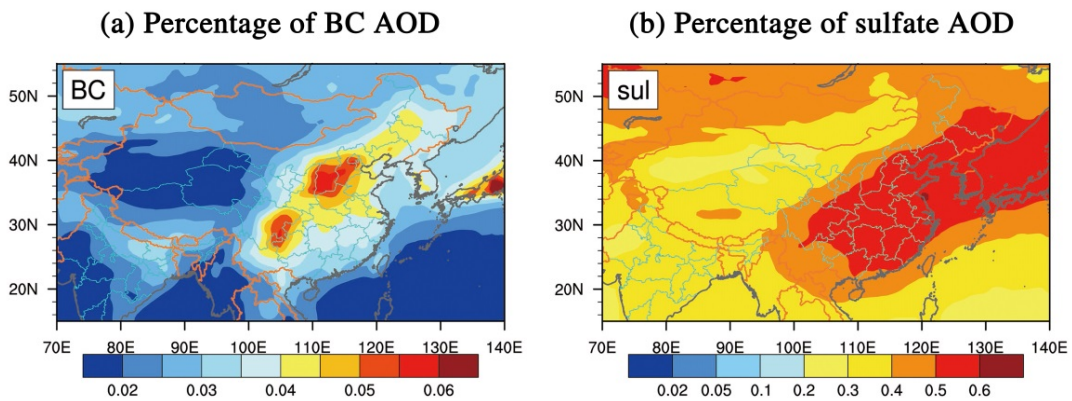
910 Figure 3. PDF of (a) start time (units: LST), (b) peak time (units: LST), and (c) duration (units: hours) of  
 911 heavy rainfall on the days that SAI more than 75<sup>th</sup> tercile (blue lines) and days that AAI more than 75<sup>th</sup> tercile  
 912 (red lines), during early summers from 2005 to 2012. The differences between two groups have all passed the  
 913 significant test of 95%.

914

915

916

917

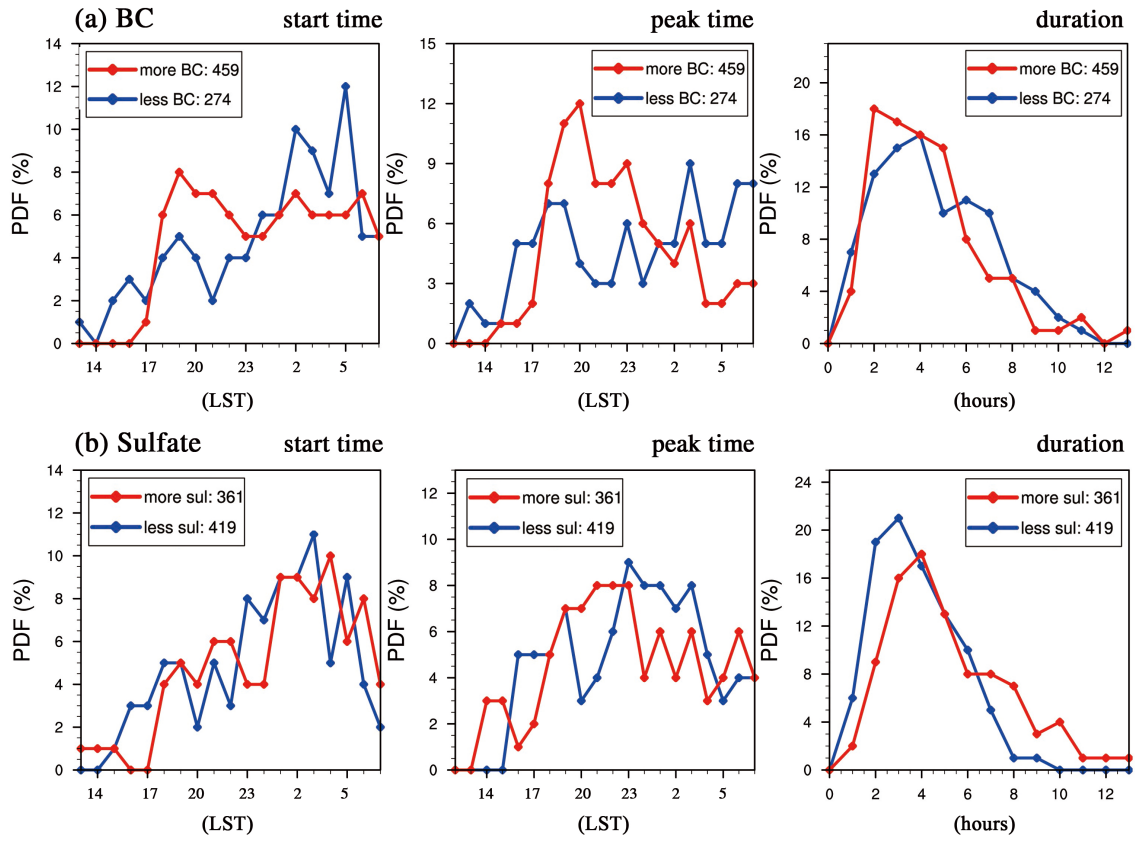


918

919 Figure 4. Percentages of AOD for (a) BC and (b) sulfate in JJA during 2002 to 2012.

920

921



922

923 Figure 5. PDF of start time (units: LST), peak time (units: LST) and duration (units: hours) of heavy rainfall in  
 924 different conditions of (a) BC and (b) sulfate. Blue/red lines stand for the condition of less/more BC or sulfate  
 925 during early summers from 2003 to 2012. The differences have passed the significant test of 95%.

926

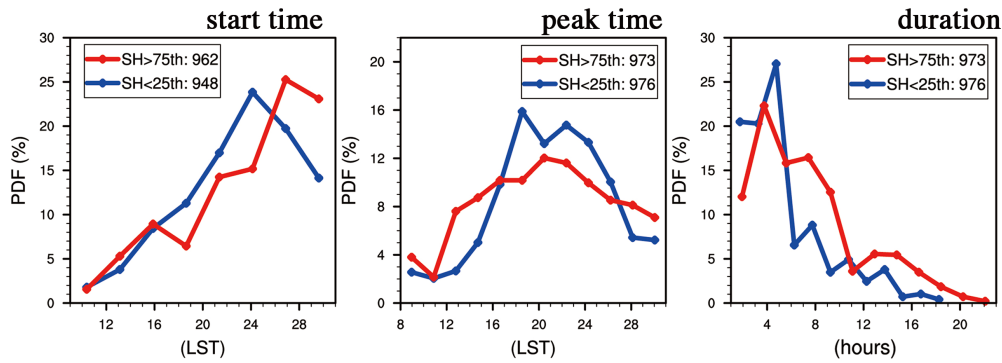
927

928

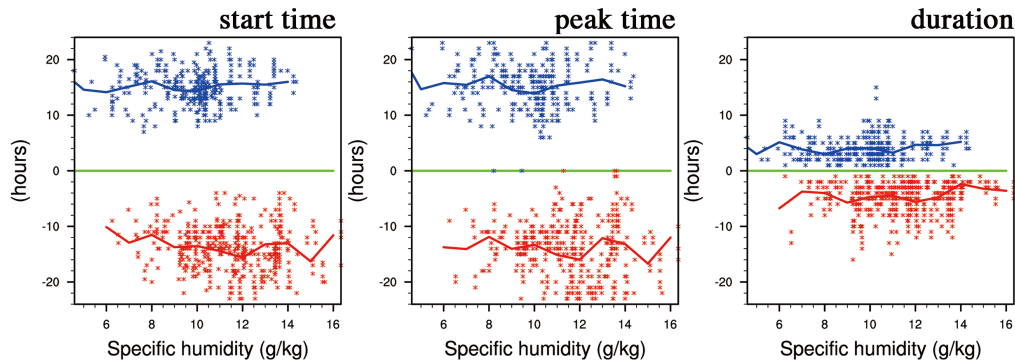
929

930

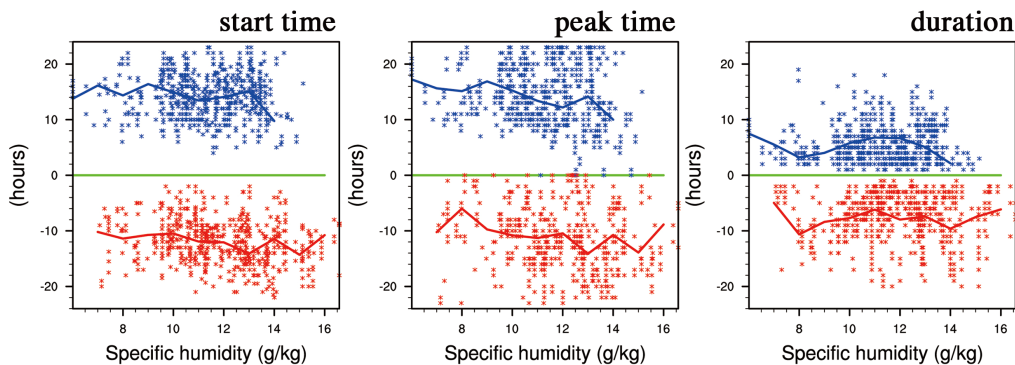
(a) PDF with more/less SH



(b) Scatter distribution using AOD



(c) Scatter distribution using CDNC



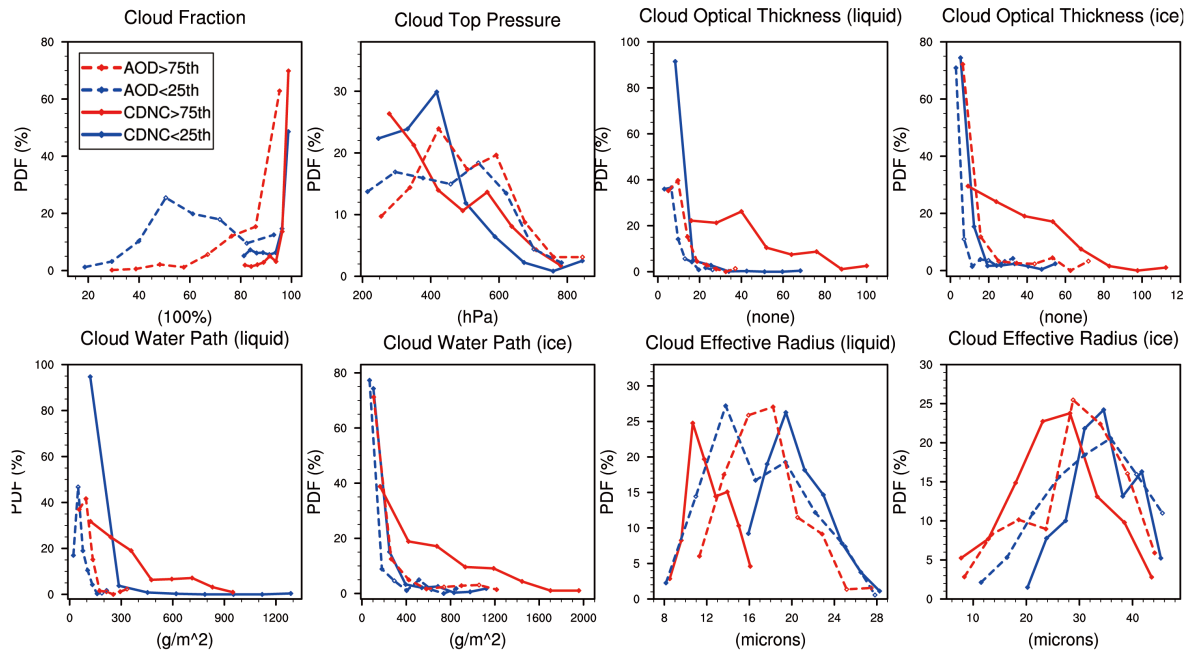
931

932 Figure 6. (a) PDF of start time (units: LST), peak time (units: LST), and duration (units: hours) of heavy  
 933 rainfall in different conditions of less moisture (blue lines, SH at 850 hPa less than 25<sup>th</sup> tercile) and more  
 934 moisture (red lines, SH at 850 hPa more than 75<sup>th</sup> tercile). (b) and (c) are scatter distributions of SH-start  
 935 time/peak time/duration for clean cases (blue points) and polluted cases (red points) respectively using AOD  
 936 and CDNC. Green lines stands for the start/peak time at 8:00 LST or duration is 0 hours. Positive (negative)  
 937 values stand for the hours away from 8:00 LST or 0 hours in clean (polluted) cases. Blue (red) lines stand for  
 938 the mean values of rainfall characteristics at each integer of SH in clean (polluted) cases.

939

940

941



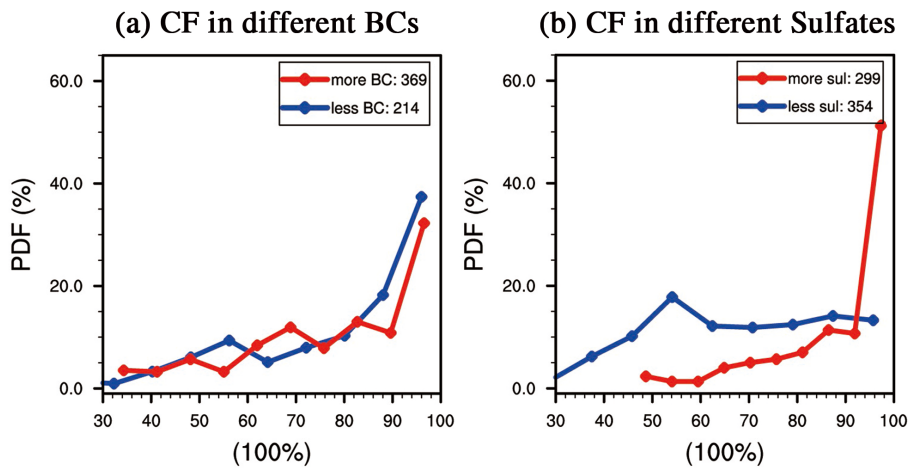
942

943 Figure 7. PDF of CF (units: %), CTP (units: hPa), COT (liquid and ice, units: none), CWP (liquid and ice,  
 944 units:  $\text{g/m}^2$ ) and CER (liquid and ice, units:  $\mu\text{m}$ ) on selected clean (blue dash lines: AOD < 25<sup>th</sup> tercile; blue  
 945 solid lines: CDNC < 25<sup>th</sup> tercile) and polluted (red dash lines: AOD > 75<sup>th</sup> tercile; red solid lines: CDNC > 75<sup>th</sup>  
 946 tercile) heavy rainfall days. The differences between clean and polluted cases have all passed the significant  
 947 test of 95%.

948

949

950



951

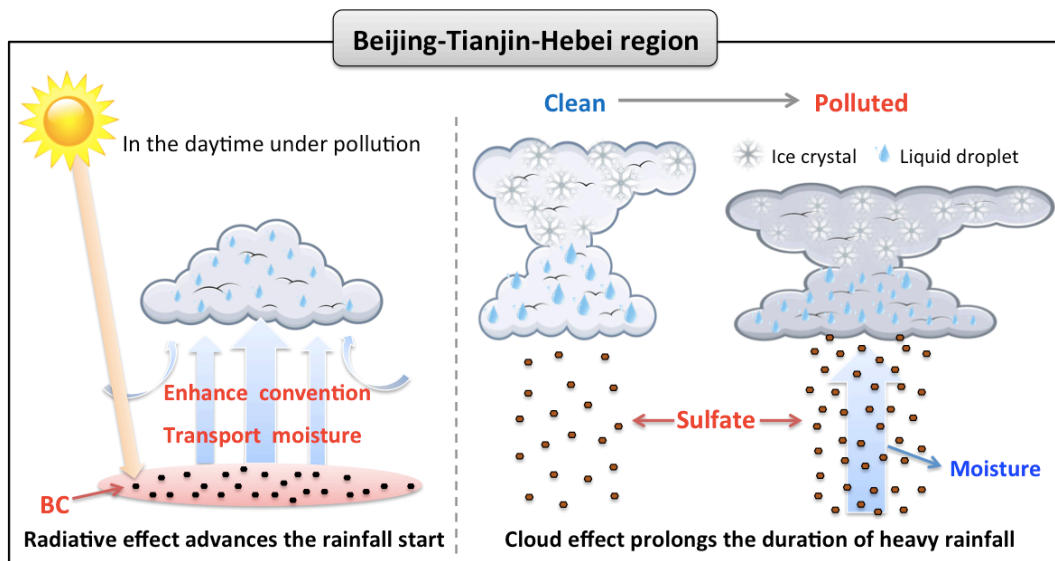
952 Figure 8. PDF of CF (units: 100%) respectively for selected less BC/sulfate (blue lines) and more BC/sulfate  
 953 (red lines) cases with heavy rainfall during 10 early summers (2003-2012).

954

955



956



957

958 Figure 9. A schematic diagram for aerosols impact on heavy rainfall over Beijing-Tianjin-Hebei region.

959

960

961